AD_____

Award Number: W81XWH-06-1-0210

TITLE: Noninvasive Localization of Prostate Cancer via Diffusion Sensitive MRI

PRINCIPAL INVESTIGATOR: Junqian Xu, Ph.D.

CONTRACTING ORGANIZATION: Washington University
St. Louis, MO 63110

REPORT DATE: March 2008

TYPE OF REPORT: Annual Summary

PREPARED FOR: U.S. Army Medical Research and Materiel Command
Fort Detrick, Maryland 21702-5012

REPORT DOCUMENTATION PAGE

Form Approved
OMB No. 0704-0188

1. REPORT DATE	2. REPORT TYPE	3. DATES COVERED
01-03-2008	Annual Summary	15 Feb 2007– 14 Feb 2008

4. TITLE AND SUBTITLE

Noninvasive Localization of Prostate Cancer via Diffusion Sensitive MRI

5a. CONTRACT NUMBER

5b. GRANT NUMBER
W81XWH-06-1-0210

5c. PROGRAM ELEMENT NUMBER

6. AUTHOR(S)

Junqian Xu, Ph.D.

Email: jxu@wustl.edu

5d. PROJECT NUMBER

5e. TASK NUMBER

5f. WORK UNIT NUMBER

7. PERFORMING ORGANIZATION NAME(S) AND ADDRESS(ES)

Washington University
St. Louis, MO 63110

8. PERFORMING ORGANIZATION REPORT NUMBER

9. SPONSORING / MONITORING AGENCY NAME(S) AND ADDRESS(ES)
U.S. Army Medical Research and Materiel Command
Fort Detrick, Maryland 21702-5012

10. SPONSOR/MONITOR'S ACRONYM(S)

11. SPONSOR/MONITOR'S REPORT NUMBER(S)

12. DISTRIBUTION / AVAILABILITY STATEMENT
Approved for Public Release; Distribution Unlimited

13. SUPPLEMENTARY NOTES

14. ABSTRACT
Diffusion tensor magnetic resonance imaging (DTI) measurements of prostate cancer (PCa) were performed in vivo, in patients undergoing radical prostatectomy, and ex vivo, in the same patients' prostatectomy specimens. For the first time, the imaging data were co-registered to histological sections of the prostatectomy specimens, thereby enabling unambiguous characterization of diffusion parameters in cancerous and benign tissues. Through image co-registration and histological analysis, we have shown that increased cellularity, and thence decreased luminal spaces, in peripheral zone PCa leads to about 40 % and 50 % apparent diffusion coefficient (ADC) decrease compared to benign peripheral zone tissues in vivo and ex vivo, respectively. In contrast, no significant diffusion anisotropy differences between the cancerous and non-cancerous peripheral zone tissues were observed. The bundled fibromuscular tissues in prostate, such as stromal tissues in benign prostatic hyperplasia (BPH), exhibited high diffusion anisotropy facilitating the differentiation of PCa from BPH in central gland. A tissue classification method, combining DTI and T2w images, was proposed to provide more specific PCa detection. An ADC threshold for PCa was also established to provide unsupervised PCa localization. The PCa identified using this method correlate well with histologically identified PCa foci.

15. SUBJECT TERMS
magnetic resonance imaging (MRI), diffusion tensor imaging (DTI), apparent diffusion coefficient (ADC), diffusion anisotropy (FA), prostate carcinoma (PCa), and benign prostatic hyperplasia (BPH)

16. SECURITY CLASSIFICATION OF:			17. LIMITATION OF ABSTRACT	18. NUMBER OF PAGES	19a. NAME OF RESPONSIBLE PERSON
a. REPORT	b. ABSTRACT	c. THIS PAGE			USAMRMC
U	U	U	UU	42	19b. TELEPHONE NUMBER *(include area code)*

Table of Contents

Introduction

Current curative strategies for prostate cancer (PCa) focus on the detection and treatment of early-stage tumors (1). However, the standard method of diagnosis, transrectal ultrasound guided needle biopsy, misses 20 – 30 % of clinically significant tumors (3). Repeated negative biopsies do not guarantee that the patient is cancer free. Although magnetic resonance imaging (MRI) provides excellent soft-tissue contrast of the prostate, the standard T2-weighted (T2w) MRI is neither sensitive nor specific enough for accurate PCa localization (1, 4). In an earlier study from this laboratory, the lower water apparent diffusion coefficient (ADC) of PCa compared to benign prostate tissues markedly improved contrast of PCa *vs.* non-cancerous prostate tissue in a transgenic mouse model *in vivo (5)*. In this pre-doctoral project awarded by Department of Defense, we proposed to investigate the ADC contrast by diffusion tensor MRI (DTI) in gland confined human PCa for improved detection and localization. The ADC and diffusion anisotropy of water, parameters derived from DTI (6), reflect tissue microstructure at the micron scale and hence are sensitive to pathologic changes. This proposal is based on the **hypothesis** that the water ADC differential between PCa and benign prostate tissues will provide the desired contrast *in vivo* for noninvasive PCa detection in patients *via* diffusion sensitive MRI. The **objective** of this work is to demonstrate that tumor foci within the prostate may be accurately identified using water ADC. Diffusion sensitive MRI, as a noninvasive method, shows the potential to accurately localize tumor foci within the prostate. Our current results have an immediate **impact** in (i) enabling MRI guided targeted needle biopsy, thus, reducing the incidence of false negative results and the need for saturation biopsy, (ii) supporting focal ablation techniques, thus, reducing the need for whole prostate resection (7), and (iii) providing a tool for watchful waiting and post-therapy monitoring.

Body

Aim 1: To validate the existance and quantify the extent *in vivo* of a large (~2 fold) water ADC differential between PCa and benign human prostate tissues. This differential is expected from (i) a previous published transgenic mouse study (5), (ii) a recent study with resected human prostates (8), and (iii) preliminary human data acquired *in vivo* (9).

Task 1 has been accomplished during the first year of the funding period and has been summaried in the 2007 annual report. To recapitulate, the major achievements are:

1. The proposed image co-registration strategy was implemented to fuse *in vivo*, *ex vivo* DTI, and optical images of histology slide (2007 annual report - Fig. 1 and 2). A match of alignment (orientation and position) between histology slides and *in vivo* ADC slices in the standard *in vivo* T2w image space was achieved for purposes of translating the histology identified PCa regions onto the *in vivo* MR images (Appendix 1).

2. After image registration, cancerous and benign tissues in the peripheral zone (PZ) were translated from the histology slides onto the *in vivo* and *ex vivo* ADC maps to

determine the ADC and diffusion anisotropy values in each tissue category (2007 annual report - Fig. 3 and 4). The ADC values in PCa were consistently much lower than that in benign tissues in patients *in vivo*, and *ex vivo* prostatectomy specimens. Although no significant diffusion anisotropy differences between the cancerous and non-cancerous PZ tissues were observed, the bundled fibromuscular tissues in prostate, such as stromal tissues in benign prostatic hyperplasia (BPH), exhibited high diffusion anisotropy facilitating the differentiation of PCa from BPH in central gland.

3. An ADC threshold (mean tumor ADC + standard deviation) for PCa was established based on the results to provide unsupervised PCa localization. The PCa identified using this method correlated well with histologically identified PCa foci (Appendix 1. Fig. 6).

4. In addition to PCa and benign PZ tissues, the ADC and diffusion anisotropy values for stromal BPH and epithelial BPH were also quantified with similar approach.

Figure 1 summarizes the ADC and fractional anisotropy (FA) values for PCa, Benign PZ, stromal BPH and epithelial BPH.

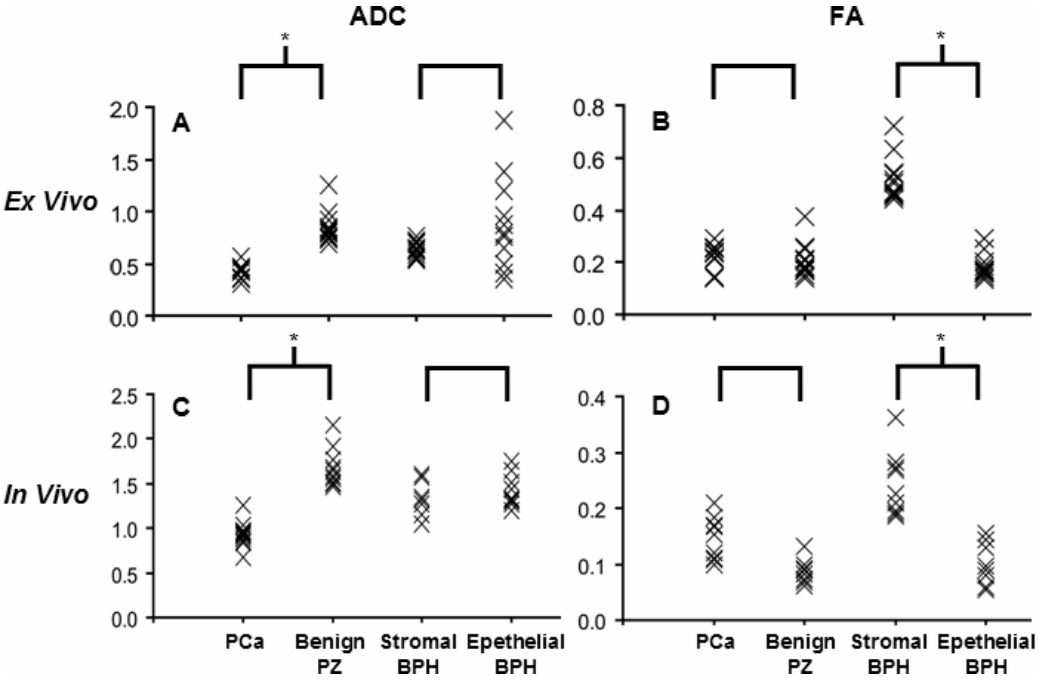

Figure 1. *Ex vivo* and *in vivo* ADC ($\mu m^2/ms$) and FA (unitless) values for each tissue type: (from left to right in each panel) PCa, benign PZ, stromal BPH, and epithelial BPH. * indicates significant differences ($p<0.01$).

We present a prostate tissue classification method that combines both DTI and T2w contrasts (Table 1). The various tissue types contributing to the classification scheme were verified by histological analysis after co-registration. In general, ADC contrast parallels the T2w contrasts with ADC being more specific than T2w contrast for

PZ PCa (Figs. 2a, b white arrows). Diffusion anisotropy provides a unique contrast that differentiates PCa from stromal BPH in the CG, while its usage for PZ PCa is limited.

		ADC	FA	T2w
PZ	PCa	hypo	iso	hypo
	Benign	-	-	-
CG	PCa	hypo	iso	hypo
	Stromal BPH	hypo	hyper	hypo
	Epithelial BPH	hetero	iso	hetero
	Benign	-	-	-

Table 1. Tissue type classification combining DTI and T2w contrasts. Benign tissues (-) in PZ and CG, respectively, were used as benchmarks for MR contrasts. MR image contrasts were listed as hypo(intense), iso(intense), hyper(intense) or hetero(geneous).

In summary, through histology analysis and image co-registration, we have validated the existance and quantified the extent of a large (~ 2 fold) water ADC differential between PCa and benign peripheral zone human prostate tissues *in vivo.* The diffusion anisotropy, derived from DTI, was also quantified in prostate through the analysis. Combining DTI and T2w contrasts has the potential to provide more specific PCa detection and accurate PCa localization.

Aim 2: To quantify the accuracy of *in vivo* ADC-based MRI tumor detection (volume) and localization (coordinate), the *in vivo* human MRI data will be compared with very high signal-to-noise/resolution MRI data acquired on the same prostate following resection and with histolgic analysis by a clinical pathologist.

In vivo diffusion MRI of the human prostate is technically challenging for reasons such as the small size of the prostate, the central location of the prostate deep within the body, the presence of interfering MR signal from fat surrounding the prostate, and the image blurring that results from respiratory motion. Image distortion and blurring commonly corrupt diffusion weighted images (DWI) of the prostate and consequently the calculated ADC map (2007 annual report - Fig. 5). Previously a phased-array body coil was used for MR signal reception. Although image distortion is, in principle, minimal with a body coil, low signal-to-noise ratio (SNR) limits achievable image resolution even with a prolonged scan time approaching 30 min. Furthermore, a lengthy acquisition leads to image blurring because of patient motion. The tumor detection limit is inherently determined by image resolution (previously $2 \times 2 \times 2.5$ mm^3 in Aim 1). During the second year of the funding period, significant effort was put into optimizing the high resolution ($1.5 \times 1.5 \times 3$ mm^3) *in vivo* diffusion MRI protocol (within a clinically acceptable 10-min acquisition time) using an endo-rectal coil to take advantage of its high SNR. Three radical prostatectomy patients were scanned with this endorectal coil protocoal at a 1.5-tesla scanner.

(A) High resolution *in vivo* inner volume diffusion MRI optimization with endo-rectal coil in receive only mode.

A challenge with using endo-rectal coil is that the inserted coil can cause magnetic susceptibility induced artifacts. These significantly distort the diffusion image. We have implemented an inner volume imaging diffusion sequence with "zoom-in" ability that significantly reduces image distortion. In the same time, it eliminates the need for the body coil during reception and, hence, results in less noise contamination. The sequence diagram and the magnetization evolution (Fig. 2) are briefly described below.

Diffusion weighting with single shot fast spin-echo (FSE) and single shot spin-echo echo planar imaging (SE-EPI) modules have been previously used to image prostate (10, 11). Due to its high SNR efficiency, SE-EPI is the sequence of choice among most research groups. In order to improve image resolution while reducing image distortion of EPI sequence, on the basis of SE-EPI, the inner volume imaging (IVI) or reduced field of view (rFOV) technique (12-16) has been recently presented. The original version of IVI technique used one 90° slice selective excitation pulse and one 180° slab selective refocusing pulse in orthogonal directions to select a rectangular volume of interest (17). The disadvantage of the original IVI technique is its low imaging efficiency because the magnetization outside of the selected slab was inverted by the 180° pulse. This makes interleaved multi-slice data acquisition problematic. Zonal oblique multislice (ZOOM) EPI method, a modified IVI technique applying the selective pulses in oblique angles (18), was developed enabling the interleaved multi-slice acquisition with judicious selections of oblique angles. This technique has been employed with diffusion encoding (12). However, ZOOM-EPI leaves slice gaps in the anatomy of interest because spatial saturation pulses were required to ensure a rectangular volume excitation. Interleaving slice groups can provide continuous coverage with loss in imaging efficiency. A solution to this shortcoming is to apply a second slab selective 180° pulse

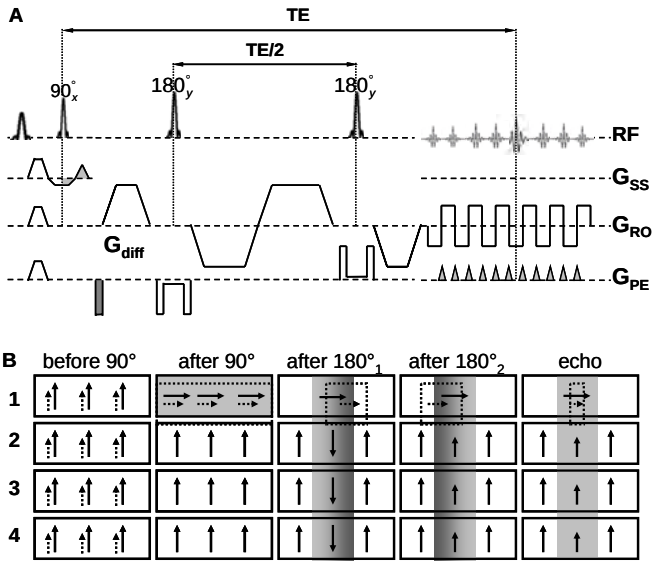

Figure 2. The top panel (A) shows a single shot SE-EPI sequence implemented with inner volume imaging (IVI) and twice refocused spin echo (TRSE) diffusion weighting. Note the 180° pulses are selective in the phase encoding (G_{pe}) direction. The direction of the diffusion sensitive gradients (G_{diff}) is arbitrary. The bottom panel (B) illustrates the magnetization evolution (adapted from Figure 1b in Jeong et al (2)) with gradient reversal technique. The shaded boxes represent the excited/refocused water slice/slab while the dashed boxes represent shifted fat slice/slab . The solid arrows and dashed arrows represent water and residual fat magnetization due to imperfect fat saturation, respectively. The fat signal (only the slice of interest is shown after the 90° excitation pulse) is greatly decreased at the time of echo formation. The effectiveness of the gradient reversal technique increases with the ratio of fat-water frequency difference to the bandwidth of the slab selective 180° refocusing/inversion pulses.

at the end of the imaging module (2). This second selective 180° pulse has the effect of restoring the magnetization inverted by the first 180° pulse back to the positive B_0 field axis before subsequent slice selective excitations. This technique was further coupled with twice refocusing spin echo (TRSE) (19) diffusion weighting scheme (Fig. 2) for diffusion measurements (16, 20) in human prostate during the second year of the funding period.

As a result of the improved image resolution and less distortion, the intraglandular features and contrast in the ADC and FA map (Fig. 3) reflected that seen in the ultra-high resolution T2W image (Fig. 3B). Importantly in this case, it is difficult to distinguish PCa from benign prostatic hyperplasia (BPH) on the basis of changes in ADC alone because both pathologies affect this diffusion parameter. An alternative means of distinguishing PCa and BPH exploits diffusion anisotropy as an auxiliary criterion. High diffusion anisotropy (FA), as indicated dark arrows in Fig. 2B, serves as an additional PCa **exclusion** criterion in the central gland and, thus, aids in identifying BPH regions that mimic PCa contrast in both the *in vivo* ADC map (Fig. 2A) and conventional T2W image (Fig. 2C). Achieving such high-quality diffusion images also improves tumor detection limit.

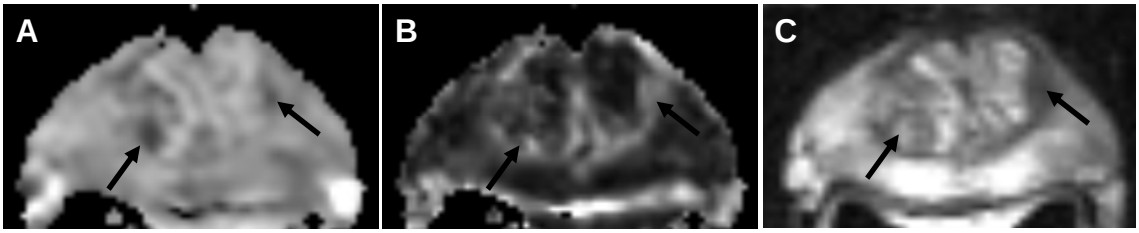

Figure 3. Co-registered images illustrate the high SNR and minimal distortion in DTI images compared to the T2w image. A) *in vivo* ADC, B) *in vivo* FA, C) *in vivo* T2W.

(A) Tumor detection limit

Taking advantage of the data acquired in Aim 1, there were a total of 67 tumor foci (median size 1.31 cc, range 0.51 - 5.05 cc) identified in histological samples from 24 patients' prostate specimens. Among all tumor foci, three groups were identified according to the size: less than 0.1 cc (n = 37), between 0.1 cc and 0.5 cc (n = 13), and greater than 0.5 cc (n = 17).

A tumor size threshold of 0.1 cc was empirically determined as the minimum size to reliably map cancerous tissue regions from histology to MR images. Hence tumor foci smaller than 0.1 cc were not mapped. This threshold excluded 37 tumor foci from the total of 67 tumor foci. In consequence, eight patients with tumor burden < 5% were excluded from further analysis, which resulted in 12 *in vivo* cases for the purpose of evaluating detection limit. The tumor sizes were then determined by counting the pixels in each identified PCa foci from histology. The tumor dimensions were also measured. The length and width were determined by averaging the two largest axes of tumor foci from all involved histology slides. The thickness of the tumor foci was determined by the product of the number of histology slides involved and the thickness of the histology section (4 mm). Table 2 summarizes the tumor foci size and dimension.

	Tumor Size (cc)	Tumor Dimension (L × W × T mm^3)
Subject 1	0.18	5.3x3.1x16
	0.13	3.8x1.8x20
Subject 2	1.47	10.8x7.0x24
	0.12	9.6x2.7x8
Subject 3	0.43	5.9x4.5x20
Subject 4	0.72	13.5x4.3x24
	0.36	10.2x2.6x28
Subject 5	0.86	14.4x8.5x8
	0.73	19.8x5.9x8
	0.16	6.3x4.1x8
Subject 6	4.07	17.6x10.0x28
	0.26	5.3x3.3x16
Subject 7	4.25	17.5x12.3x24
Subject 8	5.05	19.0x13.8x28
	0.51	10.7x3.2x20
Subject 9	1.33	21.1x12.8x8
	0.15	10.3x3.4x8
	0.11	10.7x4.1x4
Subject 10	1.03	12.0x6.7x16
Subject 11	0.9	13.8x5.4x16
Subject 12	1.32	11.6x6.3x20
	0.83	10.0x5.0x20

Table 2. Summary of tumor size and tumor dimension from 12 patients with tumor foci > 0.1 cc)

After applying the ADC threshold (mean tumor ADC + standard deviation = 1.08 $\mu m^2/ms$) as determined from Aim 1 for unsupervised PCa identification, the minimum size of the identifiable tumor is 0.36 cc. Hence the detection limit is estimated to be ~ 0.4 cc for a diffusion imaging resolution of $2 \times 2 \times 2.5$ mm^3. Unfortunately, not enough samples were acquired with the high resolution ($1.5 \times 1.5 \times 3$ mm^3) endorectal coil imaging protocol. However, based on the much improved image quality (Fig. 3), we speculate a detection limit of 0.25 - 0.3 cc is achievable *in vivo*. Noticeably, prostate tumor foci often exhibited finger like projection (table 2), i.e., irregular and anisotropic tumor dimension. Hence we emphasize the importance of a high resolution diffusion imaging protocol for accurate PCa localization for patients with small to medium sized tumor, who will benefit most from the technique developed in this research proposal.

In summary, we have achieved high resolution *in vivo* inner volume diffusion images with an endorectal coil for tumor localization in a clinically acceptable scan time. Our established *in/ex vivo* MRI and histology co-registration scheme enables us to explore the *in vivo* tumor detection limit. Our preliminary data suggested a tumor detection limit of about 0.3 - 0.4 cc with our current *in vivo* diffusion imaging protocol.

Key Research Accomplishments

1. For the first time, the imaging data were co-registered to histological sections of the prostatectomy specimens, thereby enabling unambiguous characterization of diffusion parameters in cancerous and benign tissues. Through image co-registration and histological analysis, we have shown that increased cellularity, and hence decreased luminal spaces, in peripheral zone PCa leads to ~ 40 % and 50 % ADC decrease compared to benign peripheral zone tissues *in vivo* and *ex vivo*, respectively.

2. No significant diffusion anisotropy differences between the cancerous and non-cancerous peripheral zone tissues were observed.

3. The bundled fibromuscular tissues in prostate, such as stromal tissues in benign prostatic hyperplasia (BPH), exhibited high diffusion anisotropy facilitating the differentiation of PCa from BPH in central gland.

4. An ADC threshold for PCa was established to provide unsupervised PCa localization. The PCa identified using this method correlate well with histologically identified PCa foci.

5. A tissue classification method, combining DTI and T2w images, was proposed to provide more specific PCa detection.

6. The *in vivo* diffusion image quality was significantly improved by using an endo-rectal coil and an optimized diffusion sequence/protocol developed by the trainee. As a result, the improved SNR, reduced image distortion and blurring, as well as the reduction in scan time will have significant impact on the upcoming study.

7. The tumor detection limit was estimated to be about 0.4 cc for our current diffusion imaging resolution of $2 \times 2 \times 2.5$ mm^3.

Reportable Outcomes

1. Manuscript, Abstract, and ISMRM Young Investigator Award (YIA) Finalist Oral Presentation "Magnetic Resonance Diffusion Characteristics of Histologically Defined Prostate Cancer in Human" **J. Xu**, P. A. Humphrey, A. S. Kibel, A. Z. Snyder, V. R. Narra, J. J. H. Ackerman, and S. K. Song *Magn. Reson. Med.*, accepted 2008 (previous submission, as cited in 2007 annual report, to *Cancer Research* was rejected), *Proc. Intl. Soc. Magn. Reson. Med.* accepted **16**, 2008, YIA competition during ISMRM 16th annual meeting, Toronto, Canada, May 2008,

2. Employment based on the MRI experiences supported by this award Post-doctoral fellow, Department of Neurology, Washington University in St. Louis

3. Research opportunity received based on the *in vivo* human diffusion MRI experiences supported by this award National Multiple Sclerosis Society (NMSS) post-doctoral fellowship, titled "Quantification of Spinal Cord Injury *via* diffusion MRI", FG 1782-A-1 **Xu** (PI)

4. Degree Ph.D. in Chemistry, Washington University in St. Louis, Missouri 2007

5. Abstract and Poster Presentation "Noninvasive Localization of Prostate Cancer via Diffusion-sensitive MRI" **J. Xu**, P. A. Humphrey, A. S. Kibel, A. Z. Snyder, V. R. Narra, and S. K. Song. *IMPaCT,* P30-16, 2007

6. Abstract and Electronic-Poster Presentation "ADC Decrease in Histology Identified Prostate Cancer" **J. Xu**, P. A. Humphrey, A. S. Kibel, A. Z. Snyder, V. R. Narra, and S. K. Song. *Proc. Intl. Soc. Magn. Reson. Med.* **15**, 3666, 2007

7. Abstract and Oral Presentation "Exclusion of False Positive Identification of Prostate Cancer Using Diffusion Anisotropy" **J. Xu**, P. A. Humphrey, A. S. Kibel, V. R. Narra, and S. K. Song. *Proc. Intl. Soc. Magn. Reson. Med.* **14**, 174, 2006

Conclusion

The contrast provided by diffusion sensitive magnetic resonance (MR) in organ-confined human prostate cancer (PCa) offers the promise of improved detection and localization. Diffusion tensor imaging (DTI) measurements of PCa were performed *in vivo,* in patients undergoing radical prostatectomy, and later, *ex vivo,* in the same patients' prostatectomy specimens. The imaging data were co-registered to histological sections of the prostatectomy specimens, thereby enabling unambiguous characterization of diffusion parameters in cancerous and benign tissues. Increased cellularity, and hence decreased luminal spaces, in peripheral zone PCa led to about 40% and 50% ADC decrease compared to benign peripheral zone tissues *in vivo* and *ex vivo*, respectively. In contrast, no significant diffusion anisotropy differences were observed between the cancerous and non-cancerous peripheral zone tissues. However, the dense fibromuscular tissues in prostate, such as stromal tissues in benign prostatic hyperplasia (BPH) in central gland, exhibited high diffusion anisotropy. A tissue classification method is proposed to combine DTI and T2-weighted image contrasts that may provide improved specificity of PCa detection than T2-weighted imaging alone. PCa identified in volume rendered MR images qualitatively correlates well with histologically determined PCa foci. A tumor detection limit of 0.3-0.4 cc was estimated with the current diffusion imaging protocol. A high resolution optimized diffusion imaging protocol is crutial for accurate PCa localization for patients with small to medium sized tumor, who will benefit most from the technique developed in this research proposal.

<u>IMPACT:</u>

The results obtained from this research provided solid histological evidences for the diffusion contrasts (both ADC and FA) of different prostate tissues. The quantitative values will guide future research to determine optimum ADC threshold for different patient groups with receiver operator curve (ROC) analysis. The estimated *in vivo* tumor detection limit have an immediate **impact** in patient stratification for (i) targeted needle biopsy, thus, reducing the incidence of false negative results and the need for saturation biopsy, (ii) focal ablation techniques, thus, reducing the need for whole prostate resection (7), and (iii) watchful waiting and post-therapy monitoring.

References

1. Kantoff, P. W., Rarroll, P. R., and D'Amico, A. V. (eds.) Prostate Cancer: Principles & Practice, 1st edition, p. 278-280. Philadelphia: Lippincontt Williams & Wilkins, 2002.
2. Jeong, E. K., Kim, S. E., Guo, J., Kholmovski, E. G., and Parker, D. L. High-resolution DTI with 2D interleaved multislice reduced FOV single-shot diffusion-weighted EPI (2D ss-rFOV-DWEPI). Magn Reson Med, *54:* 1575-1579, 2005.
3. Keetch, D. W., Catalona, W. J., and Smith, D. S. Serial prostatic biopsies in men with persistently elevated serum prostate specific antigen values. J Urol, *151:* 1571-1574, 1994.
4. Coakley, F. V., Qayyum, A., and Kurhanewicz, J. Magnetic resonance imaging and spectroscopic imaging of prostate cancer. J Urol, *170:* S69-75; discussion S75-66, 2003.
5. Song, S. K., Qu, Z., Garabedian, E. M., Gordon, J. I., Milbrandt, J., and Ackerman, J. J. Improved magnetic resonance imaging detection of prostate cancer in a transgenic mouse model. Cancer Res, *62:* 1555-1558, 2002.
6. Basser, P. J. and Pierpaoli, C. Microstructural and physiological features of tissues elucidated by quantitative-diffusion-tensor MRI. J Magn Reson B, *111:* 209-219, 1996.
7. Katz, A. E. and Rewcastle, J. C. The current and potential role of cryoablation as a primary therapy for localized prostate cancer. Curr Oncol Rep, *5:* 231-238, 2003.
8. Xu, J., Humphrey, P. A., Kibel, A. S., and Song, S. K. Detection and Localization of Prostate Carcinoma and Benign Prostatic Hyperplasia using DTI. Proceedings of the International Society for Magnetic Resonance in Medicine, *12:* 2508, 2004.
9. Xu, J., Humphrey, P. A., Kibel, A. S., Narra, V. R., Ackerman, J. J., and Song, S. K. In vivo Detection and Localization of Prostate Carcinoma using DTI. Proceedings of the International Society for Magnetic Resonance in Medicine, *13:* 2125, 2005.
10. Kurhanewicz, J., Vigneron, D., Carroll, P., and Coakley, F. Multiparametric magnetic resonance imaging in prostate cancer: present and future. Curr Opin Urol, *18:* 71-77, 2008.
11. Mazaheri, Y., Shukla-Dave, A., Hricak, H., Fine, S. W., Zhang, J., Inurrigarro, G., Moskowitz, C. S., Ishill, N. M., Reuter, V. E., Touijer, K., Zakian, K. L., and

Koutcher, J. A. Prostate cancer: identification with combined diffusion-weighted MR imaging and 3D 1H MR spectroscopic imaging--correlation with pathologic findings. Radiology, *246:* 480-488, 2008.

12. Wheeler-Kingshott, C. A., Parker, G. J., Symms, M. R., Hickman, S. J., Tofts, P. S., Miller, D. H., and Barker, G. J. ADC mapping of the human optic nerve: increased resolution, coverage, and reliability with CSF-suppressed ZOOM-EPI. Magn Reson Med, *47:* 24-31, 2002.
13. Hickman, S. J., Wheeler-Kingshott, C. A., Jones, S. J., Miszkiel, K. A., Barker, G. J., Plant, G. T., and Miller, D. H. Optic nerve diffusion measurement from diffusion-weighted imaging in optic neuritis. AJNR Am J Neuroradiol, *26:* 951-956, 2005.
14. Trip, S. A., Wheeler-Kingshott, C., Jones, S. J., Li, W. Y., Barker, G. J., Thompson, A. J., Plant, G. T., and Miller, D. H. Optic nerve diffusion tensor imaging in optic neuritis. Neuroimage, *30:* 498-505, 2006.
15. Wheeler-Kingshott, C. A., Trip, S. A., Symms, M. R., Parker, G. J., Barker, G. J., and Miller, D. H. In vivo diffusion tensor imaging of the human optic nerve: pilot study in normal controls. Magn Reson Med, *56:* 446-451, 2006.
16. Xu, J., Naismith, R. T., Trinkaus, K. M., Cross, A. H., and Song, S. K. Towards Accurate In Vivo Diffusion Measurement in Human Optic Nerve. *In:* Proceedings of the 15th Annual Meeting of ISMRM, Berlin, Germany, 2007, pp. 11.
17. Feinberg, D. A., Hoenninger, J. C., Crooks, L. E., Kaufman, L., Watts, J. C., and Arakawa, M. Inner volume MR imaging: technical concepts and their application. Radiology, *156:* 743-747, 1985.
18. Weaver, J. B., Harris, R. D., and Spiegel, P. K. Limited field of view spin echo MR imaging. Magn Reson Imaging, *9:* 389-394, 1991.
19. Reese, T. G., Heid, O., Weisskoff, R. M., and Wedeen, V. J. Reduction of eddy-current-induced distortion in diffusion MRI using a twice-refocused spin echo. Magn Reson Med, *49:* 177-182, 2003.
20. Dowell, N. G., Miller, D. H., Jenkins, T., and Wheeler-Kingshott, C. Contiguous-Slice Diffusion Tensor Imaging of the Optic Nerve with CSF Suppressed IR CO-ZOOM. *In:* Proceedings of the 15th Annual Meeting of ISMRM, Berlin, Germany, 2007, pp. 10.

Appendices

1. Manuscript, Abstract, and ISMRM Young Investigator Award (YIA) Finalist Oral Presentation "Magnetic Resonance Diffusion Characteristics of Histologically Defined Prostate Cancer in Human" **J. Xu**, P. A. Humphrey, A. S. Kibel, A. Z. Snyder, V. R. Narra, J. J. H. Ackerman, and S. K. Song *Magn. Reson. Med.*, accepted 2008 (previously submission, as cited in 2007 annual report, to *Cancer Research* was rejected), *Proc. Intl. Soc. Magn. Reson. Med.* accepted **16**, 2008, YIA competition during ISMRM 16th annual meeting, Toronto, Canada, May 2008,

2. Abstract and Electronic-Poster Presentation "ADC Decrease in Histology Identified Prostate Cancer" **J. Xu**, P. A. Humphrey, A. S. Kibel, A. Z. Snyder, V. R. Narra, and S. K. Song. *Proc. Intl. Soc. Magn. Reson. Med.* **15**, 3666, 2007

3. Abstract and Oral Presentation "Exclusion of False Positive Identification of Prostate Cancer Using Diffusion Anisotropy" **J. Xu**, P. A. Humphrey, A. S. Kibel, V. R. Narra, and S. K. Song. *Proc. Intl. Soc. Magn. Reson. Med.* **14**, 174, 2006

Magnetic Resonance Diffusion Characteristics of Histologically Defined Prostate Cancer in Humans

Junqian Xu,[1] Peter A. Humphrey,[2] Adam S. Kibel,[3,4,8] Abraham Z. Snyder,[5,6] Vamsidhar R. Narra,[5] Joseph J. H. Ackerman,[1,5,7,8] and Sheng-Kwei Song[5]

Departments of [1]Chemistry, [2]Pathology and Immunology, [3]Surgery, [4]Genetics, [5]Radiology, [6]Neurology, [7]Internal Medicine, and [8]Siteman Cancer Center, Washington University, One Brookings Drive, St. Louis, MO 63130

Grant support: This study was supported, in part, by the Washington University Small Animal Imaging Resource - a National Cancer Institute funded Small Animal Imaging Resource Program facility R24 CA83060, the Small Animal Imaging Core of the Alvin J. Siteman Cancer Center - a National Cancer Institute Comprehensive Cancer Center P30 CA91842, the NINDS center core grant NS048056, the U.S. Army Department of Defense Prostate Cancer Program Predoctoral Fellowship PC050667, and the Midwest Stone Institute.

Note: Preliminary reports of this work may be found in the Proceedings of the 12-15th Annual Meeting of International Society for Magnetic Resonance in Medicine. 2004. p. 2508, 2005. p. 2125, 2006. p. 174, and 2007. p. 3666.

Running Title

MR Diffusion Characteristics of PCa

Requests for reprints: Sheng-Kwei Song, Biomedical MR Laboratory, Department of Radiology, Campus Box 8227, Washington University School of Medicine, 4525 Scott Avenue, St. Louis, MO 63110. Phone: (314) 362-9988; Fax: (314) 362-0526; E-mail: ssong@wustl.edu.

Full Papers: 4042 words, 6 figures and tables, 34 citations

ABSTRACT

The contrast provided by diffusion sensitive magnetic resonance (MR) in organ-confined human prostate cancer (PCa) offers the promise of improved detection and localization. Diffusion tensor imaging (DTI) measurements of PCa were performed *in vivo*, in patients undergoing radical prostatectomy, and later, *ex vivo*, in the same patients' prostatectomy specimens. The imaging data were co-registered to histological sections of the prostatectomy specimens, thereby enabling unambiguous characterization of diffusion parameters in cancerous and benign tissues. Increased cellularity, and hence decreased luminal spaces, in peripheral zone PCa led to about 40% and 50% ADC decrease compared to benign peripheral zone tissues *in vivo* and *ex vivo*, respectively. In contrast, no significant diffusion anisotropy differences were observed between the cancerous and non-cancerous peripheral zone tissues. However, the dense fibromuscular tissues in prostate, such as stromal tissues in benign prostatic hyperplasia (BPH) in central gland, exhibited high diffusion anisotropy. A tissue classification method is proposed to combine DTI and T2-weighted image contrasts that may provide improved specificity of PCa detection than T2-weighted imaging alone. PCa identified in volume rendered MR images qualitatively correlates well with histologically determined PCa foci.

KEY WORDS

prostate carcinoma (PCa), diffusion tensor imaging (DTI), apparent diffusion coefficient (ADC), fractional anisotropy (FA)

INTRODUCTION

Prostate cancer (PCa) is the leading malignancy and the second most common cause of cancer death in American men (1). Current curative strategies focus on the detection and treatment of early-stage tumors (2). The standard method of diagnosis, transrectal ultrasound guided needle biopsy, misses 20 – 30 % of clinically significant tumors (3). A noninvasive imaging method to accurately localize PCa could guide targeted biopsy and theoretically decrease the false negative rate of needle biopsy. In addition, accurate tumor localization within the prostate would enable focal therapies using cryosurgery (4), intensity modulated radiation therapy (IMRT) (5), brachytherapy (6), or high intensity focused ultrasound (HIFU) (7), to effect a "partial prostatectomy" (i.e., to ablate just the tumor).

Current magnetic resonance (MR) imaging evaluation of PCa primarily relies on multi-planar T2-weighted (T2w) contrast, which is not sensitive or specific enough for accurate PCa localization (2,8). Other promising MR methods are being pursued. For example, the ^{1}H MR spectroscopy (MRS) determined (choline + creatine) to citrate resonance intensity ratio has been shown to be a predictive molecular signature of PCa (9). Dynamic contrast enhanced (DCE) MRI has also been explored to evaluate the microvasculature characteristics of PCa, including vascular volume and permeability (10,11). Both MRS and DCE MRI have been used to complement T2w imaging. However, neither method currently provides the image resolution sufficient for practical tumor localization.

Diffusion sensitive MR imaging, with higher resolution than the MRS and DCE MRI, also holds promise for improved PCa localization. The apparent diffusion coefficient (ADC) and diffusion anisotropy of water, parameters derived from diffusion tensor imaging (DTI), reflect tissue microstructure at the micron scale and hence are sensitive to pathologic changes (12). In an earlier study from this laboratory, the markedly lower ADC of PCa compared to normal prostate provided greatly improved diffusion contrast of PCa *vs.* non-cancerous prostate tissue in a transgenic mouse model *in vivo* (13). The approximately 70 % ADC decrease in PCa compared to non-cancerous prostate in the mouse has its origins in the distinct micro-architectural features of these tissues. While there are significant differences between the structure of mouse and human prostate, the characteristic ductal branching morphology of normal prostate tissue and the increased cellularity in PCa are the same. Hence, the distinct

micro-architectural features leading to decreased ADC in PCa relative to non-cancerous prostate should also be present in humans.

Indeed, *in vivo* diffusion measurements of human prostate have reported a decreased ADC value in suspected cancerous tissues identified by either T2w images or biopsy results (14-21). While such findings are encouraging, discrepancies in the reported diffusion indices emphasize the circumstantial (inferential) nature of such observations. Remarkably, the expectation of significantly decreased ADC in human PCa *in vivo* has yet to be directly confirmed or quantified *via* "gold standard" PCa identification of the suspected lesions through step-section histology and co-registration. Here, for the first time, the MR diffusion characteristics of histologically defined PCa were directly determined and quantified both *in vivo,* in radical prostatectomy patients prior to surgery, and, later, *ex vivo,* in the same patients' prostatectomy specimens post resection. Quantitatively translating earlier findings in a mouse model (13), this work supports the promise of diffusion sensitive MR for the non-invasive identification and localization of PCa in man.

MATERIALS AND METHODS

Patients: Twenty four prostate cancer patients to undergo radical prostatectomy (mean age 62 years; range 46 - 76 years) were recruited for this study. Patients received any preoperative treatment such as androgen ablation or radiation therapy were excluded. This study was approved by the local Institutional Review Board. Informed consent was obtained from each patient prior to the study. The prostates from 14 patients, of which 12 had tumor size greater than 0.1 cc, were examined both *in vivo* - prior to surgery, and *ex vivo* - after resection. The prostates of the other 10 patients, of which 4 had tumor size greater than 0.1 cc, were examined only *ex vivo*, after resection. The 16 patients with tumor size greater than 0.1 cc had post-surgery histology-determined median tumor burden of 20% (range 5% to 46%) and a median post-resection Gleason score of 3 + 4 = 7 (range 3 + 3 = 6 to 4 + 5 = 9). There were a total of 67 tumor foci (median size 1.31 cc, range 0.51 - 5.05 cc) identified in histological samples from these 16 patients' prostate specimens. Among all tumor foci, three groups were identified according to the size: less than 0.1 cc (n = 37), between 0.1 cc and 0.5 cc (n = 13), and greater than 0.5 cc (n = 17). Nine of the 16 patients had peripheral zone (PZ) PCa invading the

central gland (CG) or PCa originating from the transitional zone (TZ). Benign prostatic hyperplasia (BPH) was present in all but three patients.

***In vivo* MRI:** Fourteen patients underwent DTI and conventional T2w MR imaging before surgery. *In vivo* imaging was performed on a 1.5-tesla MR scanner (Sonata, Siemens AG, Erlangen, Germany) using a four-channel body phased-array surface coil. The whole prostate gland was examined, employing both diffusion weighted (DW) and T2w multislice (2.5-mm thick transverse slices) imaging. DWI was performed using a single shot spin-echo echo planar imaging (SE-EPI) sequence with field of view (FOV) 256 × 256 mm^2, data matrix 128 × 128, partial *k*-space 6/8, TR/TE 4000/76 ms, diffusion time (Δ) 30 ms. An acceleration factor of two was used to shorten the EPI echo train length, and hence reduce off-resonance distortions, in the phase encoding direction *via* the generalized auto-calibrating partially parallel acquisition (GRAPPA) technique (22). Neither cardiac/peripheral pulse nor respiratory triggering was used. Four image datasets, each consisting of one image with *b* value of 0 s/mm^2 and six diffusion sensitized images on six non-collinear (oblique dual gradient or ODG) diffusion encoding directions with *b* values of 500 s/mm^2, were acquired and the magnitude images averaged (23). Sixteen of these averaged full DWI data sets, each post-processed to correct for artifacts resulting from eddy currents and motion, were collected and averaged to further improve the signal-to-noise ratio (SNR) (24). ADC and fractional anisotropy (FA) maps were calculated on a voxel-by-voxel basis after two-point (*i.e.*, two *b* values) logarithmic fit of the image intensity and diffusion tensor matrix diagonalization (12). The total acquisition time for *in vivo* DTI was about thirty minutes. T2w images were acquired with a turbo spin echo (TSE) sequence with FOV 256 × 256 mm^2, matrix 256 × 256, echo train length (ETL) 13, and TR/TE 2800/120 ms.

***Ex vivo* MRI:** After surgery, each prostate specimen was fixed with 10% formalin in phosphate buffered saline (PBS, pH = 7.4) for more than 48 hours. The specimen was step-sectioned at 4 mm intervals from base to apex using a laboratory designed and constructed prostate slicer. The step-sectioned slices were re-grouped into a whole prostate with thin plastic spacers placed between each 4 mm slice. The regrouped prostate specimens then were wrapped in a lint-free tissue (Kimwipes, Kimberly-Clark, GA) and placed in a formalin filled plastic bag to hold the slices in place and to prevent tissue dehydration. *Ex vivo* specimens were imaged on a 4.7-tesla MR scanner (console by Varian NMR Systems, Palo Alto, CA; magnet by Oxford Instruments, Oxford, UK; gradients by Magnex Scientific, Oxford, UK) using a 5-cm diameter

quadrature "Litzcage" radio frequency coil (Doty Scientific, Columbia, SC). A multislice spin echo imaging sequence with a pair of diffusion sensitizing pulsed gradients was employed to acquire DW images (25). High resolution (500 × 500 × 500 μm^3) images were collected with diffusion time (Δ) 12 ms, diffusion gradient duration (δ) 4 ms, slice thickness 0.5 mm, FOV 6.5 cm × 6.5 cm, data matrix 128 × 128, TR/TE 6000/35 ms. The number of obtained slices was sufficient to cover each specimen completely. Eight DW image datasets, each consisting of twelve images with two *b* values of 45 and 1130 s/mm^2 on six non-collinear (oblique dual gradient or ODG) diffusion encoding directions, were averaged in the complex *k*-space (23). The magnitude images of the averaged data were used to calculate ADC and FA maps by standard procedures as for the *in vivo* experiments (12). The total acquisition time for *ex vivo* DTI was about 12 hours. T2w images were acquired with a multi-slice SE sequence with FOV 6.5 × 6.5 mm^2, data matrix 128 × 128, and TR/TE 5000/60 ms.

Histology: After *ex vivo* MRI data was acquired, each 4-mm slice from the resected specimen was cut into halves or into quarters depending on the size of each slice and embedded in paraffin. A 4-μm slice was obtained parallel to the MR imaging plane for hematoxylin and eosin (H & E) staining. Regions of PCa and BPH were delineated in blue/black and red, respectively, on all H & E stained slides by an experienced urologic pathologist (P.A.H.) blinded to the MR imaging results. The intraglandular tumor extent, reported as volume percentage of the gland containing carcinoma, was determined by grid morphometry (26). Histology slides from half-cut or quarter-cut specimens were later digitized and reassembled together into whole cross-sectional slices. The tumor sizes were then determined by counting the pixels in each identified PCa foci. Regions of BPH containing predominantly fibromuscular or epithelial cells (minimum size 0.1 cc) were identified as stromal or epithelial BPH, respectively, by one of the author (J.X.) on the digitized slides.

MR/Histology Image Co-Registration: The specifically sliced prostatectomy specimens maintain near identical coordinate systems between *ex vivo* diffusion MR and histology. To account for histological slicing and mounting distortions, a two-dimensional (2D) thin plate spline (TPS) warping was performed using 10 – 20 control points to correct the histology image coordinates to the coordinates of *ex vivo* MR images using ImageJ (NIH, Bethesda, MD) software (27,28). Using a rigid body three-dimensional (3D) affine transformation with nine degrees of freedom (DOF), each *ex vivo* ADC and FA map was further

transformed into the coordinate of the corresponding *in vivo* T2w image based on the manual alignment of intragladular structures using the ITK registration module in Analyze (Mayo Clinic, Rochester, MN) software. The final step of co-registering the *in vivo* ADC and FA maps to the *in vivo* T2w images was accomplished by using an unsupervised 3D affine transformation with twelve DOF with laboratory developed software (24). As summarized in Fig. 1, a match of alignment (orientation and position) between histology slides and *in vivo* ADC and FA slices in the standard *in vivo* T2w image space was achieved for purposes of mapping the histologically identified tissue types onto the *in vivo* MR images. A tumor size threshold of 0.1 cc was empirically determined as the minimum size to reliably map cancerous tissue regions from histology to MR images. Hence tumor foci smaller than 0.1 cc were not mapped. This threshold excluded 37 tumor foci from the total of 67 tumor foci. In consequence, eight patients with tumor burden < 5% were excluded from further analysis, which resulted in 16 *ex vivo* and 12 *in vivo* cases to define histology-DTI PCa correspondence. After MR and histology image co-registration for each slice, regions of the PCa, the benign tissue in the PZ, and the BPH were mapped from the histology slide to both the *ex vivo* and *in vivo* diffusion maps.

Statistical Analysis: Paired Wilcoxson rank tests were performed. Results are presented as mean ± standard deviation (SD). Statistical significance was defined as $p < 0.01$.

Volume Rendering: Representative *ex vivo* and *in vivo* DTI images were volume rendered using Amira (Mercury Computer Systems, Richmond, TX) software. The whole prostate gland was segmented from *ex vivo* or *in vivo* T2w images. The ADC and FA values were imported into yellow-orange and green-blue channels, respectively. The scales for ADC were inverted for visualization with bright yellow-orange regions in the MR images as carcinoma determined by an upper ADC threshold (mean tumor ADC + SD). The scales for FA were chosen for optimal visualization of fibromuscular tissues. For *ex vivo* cases, two dimensional (2D) projection images were taken and ejaculatory ducts were segmented from ADC map separately due to the very high ADC value of the structure (color scale reversed comparing with the prostate tissues). For *in vivo* cases, the volume rendered images were projected onto representative T2w images.

RESULTS

The ADC value of PCa tissue (0.43 ± 0.06 μm^2/ms *ex vivo*, Fig. 2d blue arrow, and 0.94 ± 0.14 μm^2/ms *in vivo*, Fig. 2a blue arrow) was significantly lower (p = 0.00048 *ex vivo*, and p = 0.0025 *in vivo*) than that of the non-cancerous PZ tissues (0.84 ± 0.13 μm^2/ms *ex vivo*, and 1.66 ± 0.21 μm^2/ms *in vivo*). The difference between ADC value of stromal BPH (0.65 ± 0.08 μm^2/ms *ex vivo*, and 1.28 ± 0.20 μm^2/ms *in vivo*) was not significant (p = 0.13 *ex vivo* n = 16, and p = 0.098 *in vivo* n = 12) from that of the epithelial BPH (0.85 ± 0.44 μm^2/ms *ex vivo*, and 1.42 ± 0.19 μm^2/ms *in vivo*).

A relatively low diffusion anisotropy was observed in the PZ. No significant diffusion anisotropy differential was observed (peripheral zone, Figs. 2c and f, Figs. 3a and c) between the cancerous and non-cancerous PZ tissues (FA = 0.23 ± 0.04 *vs.* 0.21 ± 0.06, p = 0.40 for *ex vivo* n = 16; and FA = 0.14 ± 0.04 *vs.* 0.09 ± 0.03, p= 0.018 for *in vivo* n = 12). However, when the fibromuscular cells are bundled together at a length scale comparable to MRI voxel dimensions (Fig. 2i), significantly higher (p = 0.00024 *ex vivo* n = 13, and p = 0.0039 *in vivo* n = 9) diffusion anisotropy in those regions, such as stromal BPH (FA = 0.52 ± 0.08 *ex vivo* and 0.24 ± 0.06 *in vivo*) becomes distinctive and distinguishable (red arrows, Figs. 2c and f, Figs. 3a and c, and Fig. 4d) from that in the glandular regions, such as epithelial BPH (FA = 0.18 ± 0.05 *ex vivo* and 0.08 ± 0.01 *in vivo*).

Figure 4 summarizes the ADC and FA values for PCa, Benign PZ, stromal BPH and epithelial BPH.

DISCUSSION

We present a prostate tissue classification method that combines both DTI and T2w contrasts (Table 1). The various tissue types contributing to the classification scheme were verified by histological analysis after co-registration. In general, ADC contrast parallels the T2w contrasts with ADC being more specific than T2w contrast for PZ PCa (Figs. 2a, b white arrows). Diffusion anisotropy provides a unique contrast that differentiates PCa from stromal BPH in the CG, while its usage for PZ PCa is limited.

Microscopically, normal prostate has a branching duct-acinar glandular architecture embedded in a dense fibromuscular stroma (Fig. 2g). This duct-acinar structure underlies the diffusion MR characteristics of the prostate gland in both human and the previously reported

mouse model. In prostate carcinoma, tightly packed tumor cells disrupt the duct-acinar structure leading to the decreased ADC in tumor due to the cellularity induced diffusion restriction (Fig. 2h).

The luminal space in benign human prostate is, on average, hundreds of microns wide. Under conditions typical of diffusion sensitive MR imaging protocols, as in this study with an *in vivo* diffusion time Δ of 30 ms, it is estimated that water diffuses over a distance of tens of microns. Thus, water in the normal prostate is relatively unrestricted and the ADC measured *in vivo* in humans is fairly high, typically ~ 1.7 $\mu m^2/ms$. (Note: *in vivo* ADC of ~ 0.8 $\mu m^2/ms$ has been reported in normal human brain grey or white matter.) The high cellularity of most PCa presents hindrances and restrictions to water diffusion over a distribution of length scales covering from the submicron to tens of microns range. This is the displacement scale to which the MR diffusion imaging is sensitive. Thus, the majority of PCa is found to have a markedly lower ADC *in vivo* than non-cancerous prostate. It is noteworthy that some intermediate grade (e.g., Gleason grade = 3, score = 6) infiltrative PCa does not affect the prostate cellularity; hence theoretically no change in ADC may be expected. This type of PCa may also be of significant clinical relevance and require other contrast mechanisms or modality to detect.

The nearly two fold *in vivo* ADC difference between PCa and benign prostate was preserved in formalin-fixed prostatectomy specimens, in agreement with Williams. (29). Although the formalin fixation process reduces the ADC's for both PCa and normal prostate tissue, the microstructure is largely preserved as evidenced by the comparable ADC decrease observed for PCa relative to non-cancerous prostate tissue both *in vivo* (~ 40%) and *ex vivo* (~ 50%). We speculate that further diffusion sensitive MR studies of radical prostatectomy specimens may provide a correlation between tumor grade and certain MR diffusion signature, which can be translated to *in vivo* studies.

The ADC value in the human prostate gland is not homogeneous (Fig. 2d). In normal peripheral zone tissues, ADC maps acquired *ex vivo* usually display bright spots (high ADC values) scattered throughout a relatively uniform background of somewhat lower ADC. We speculate that these high ADC voxels reflect regions with large diameter glandular spaces. This ADC heterogeneity is lost due to significant partial volume effect and hence not observed under the coarser *in vivo* MR image resolution (Fig. 2a).

The ADC distribution is even more heterogeneous in the CG, including the transition zone, spanning the complete spectrum of observable ADC values in the prostate *ex vivo* (Fig. 5e). The presence of BPH, the variation in stromal and epithelial tissue composition, and the formation of cysts in the CG all contribute to the observed wide distribution of ADC values. Regions of BPH composed of compact fibromuscular stroma exhibit low ADC values. In optical density measurements, these stromal BPH appears to be similar in tissue density to the closely packed glands in PCa (30). This is likely the cause of the overlap of ADC values between PCa and BPH. On the other hand, BPH dominated by glandular epithelial cell proliferation exhibits heterogeneous ADC contrast. Regions of sparse epithelial BPH components exhibit relatively high ADC values comparable to benign PZ tissues, while regions of compact epithelial BPH components exhibit considerably low ADC values similar to PCa. Therefore, the overall BPH ADC-contrast depends on the ratio of the stromal and epithelial components, as well as the compactness of cell packing. As the composition of BPH and CG is extremely variable and almost always heterogeneous, ADC contrast will vary significantly between different regions in the same patient's prostate and between patients.

Although such variation is less obvious *in vivo* than *ex vivo* due to increased partial volume averaging at the lower MR spatial resolution of *in vivo* images, the ADC values of BPH overlaps with both PCa and Benign PZ. The appearance of BPH in ADC map (Fig. 5e) or T2w image (Fig. 5f) is also heterogeneous within subject, reflecting the complicated BPH tissue composition. BPH regions with both ADC and T2w hypointensity could mimic PCa in the CG (Figs. 2a and b, red arrows), leading to false positive PCa identification. In such ambiguous cases, the contrast provided by diffusion anisotropy may offer a means to differentiate BPH from PCa in the central gland, which accounts for about 30 % of all PCa.

Water molecules in dense fibromuscular stroma in the prostate exhibit high diffusion anisotropy due to the anisotropic structure of smooth muscle cells. The network of fibromuscular connective tissues in the prostate leads to the observed diffusion anisotropy. Relatively high anisotropy is commonly observed *ex vivo* in the periurethral muscles, anterior fibromuscular regions, stromal BPH or fibrous tissues surrounding the BPH. The latter develops as the expanding BPH pushes and compresses the fibromuscular system around it (Fig. 5d). Stromal BPH in the CG usually displays similar ADC and T2w contrast as PCa (Figs. 1a and b, red arrow), likely attributable to the similar tissue density (30). The high diffusion anisotropy in

the bundled fibromuscular cells provides a unique contrast for differentiating these BPH nodules from PCa (Figs. 2c and f). Notably, the high diffusion anisotropy appears not only in the stromal components within BPH, but also in the fibrous tissues surrounding the BPH (Fig. 5d), as the expanding BPH nodule pushes and compacts the fibromuscular tissue network around it. This high diffusion anisotropy pattern surrounding the BPH was best visualized in the volume rendered DTI images (Fig. 5b).

However, the diffusion anisotropy is not particularly evident in the PZ with the *b* values and scale of the MR imaging resolution employed herein (Fig. 2f, Fig. 3c and Fig. 5d, PZ tissues). The low diffusion anisotropy in the PZ likely reflects the random orientation of fibromuscular cells in the PZ (Figs. 2g and h). The microscopic anisotropy in prostate is also subject to partial volume averaging. Hence, much lower diffusion anisotropy is observed *in vivo* (resolution $2 \times 2 \times 2.5$ mm^3) comparing to that of *ex vivo* (resolution $0.5 \times 0.5 \times 0.5$ mm^3). The diffusion anisotropy measurement, which reports the standard deviation of the principal diffusivities, is also sensitive to measurement noise. More specifically, the measured anisotropy is always biased upwards with the increased image noise. As SNR is always a concern for the *in vivo* diffusion imaging experiment, artifactually high diffusion anisotropy due to noise variation is not uncommon (Fig. 2c blue arrow). This is especially true in the PCa region where shorter T2 leads to significantly reduced SNR than that in the benign tissue regions (31). Microscopically, there is no histological evidence to support an increased density of fibromuscular tissues in PCa. In addition, the fibromuscular cells in PCa, like those in the benign peripheral zone tissues, do not bundle together or show a coherent orientation (Fig. 2h). Such random micro-architecture is unlikely to result in increased diffusion anisotropy under the present imaging conditions. Thus, we did not observe a significant anisotropy differential between the PCa and non-PCa peripheral zone tissues, either *ex vivo* or *in vivo*. This latter negative finding is in contrast to the positive results reported by Gibbs et al, the preliminary findings on pre and post hormone/radiation therapy PCa patients by Vigneron et al and Chen et al, respectively, where significant anisotropy contrast between these tissues were reported (21,32,33). Sinha et al reported even higher values of anisotropy (mean FA range 0.41 - 0.50) for both the peripheral zone and central gland tissue in a study of volunteers (34). Although age differences could be a confounding factor, such high diffusion anisotropy is likely due to artifactual noise variation, as reported by Reinsberg et al. who evaluated effects of SNR on diffusion anisotropy in human prostate *in vivo* (35). The low

diffusion anisotropy of PCa and non-PCa peripheral zone tissues reported in the present study are in agreement with the preliminary reports by Reinsberg et al. using an EPI diffusion sequence, Haker et al and Roebuck et al using a line-scan diffusion sequence, and Vigneron et al using a fast spin-echo diffusion sequence (33,35-37). Considering the technical constraints encountered with *in vivo* body diffusion imaging, accurate diffusion anisotropy measurement in human prostate *in vivo* remains a challenge.

The precise co-registration using histologically identified PCa employed in this study avoids the uncertainty of *in vivo* T2w image ROI placement and/or the sampling error of needle biopsy. Such methodological differences likely explain the approximately 30% lower *in vivo* PCa mean ADC value (0.99 $\mu m^2/ms$) reported herein compared to that reported for suspected PCa by others (range 1.27 - 1.43 $\mu m^2/ms$) (19). The co-registration error is a concern in the current study for the manual registration step used to translate the *ex vivo* coordinates to the *in vivo* space. Nevertheless, the patients recruited in this study (mean age 62 years) commonly harbor large amounts of BPH, and cysts. These intraglandular landmarks, easily identified in both *in vivo* T2w image, and *ex vivo* ADC or FA map, facilitated the manual co-registration procedure. Such landmarks also help to guide the placement of control points in both histology slide and corresponding *ex vivo* MR images to achieve an accurate warping of the histology slide into the *ex vivo* MR coordinate. The latter could be performed more accurately using whole mount histology slides. Additionally, the entire co-registration procedure could be optimized by using mutual information based automatic procedures such as that reported by Meyer et al (38).

A phased-array body receiver coil was used for *in vivo* MR data acquisition in this study instead of an endo-rectal receiver coil. The limited signal sensitivity of the phased-array body receiver coil for the prostate gland residing at the center of the body mandated significant signal averaging, thus, a prolonged scan time. The relatively small *b* values was employed considering factors of relatively insensitive phased array coil for signal reception, low magnetic field strength (1.5-tesla scanner), and the expected relatively high benign prostate tissue ADC. The use of an endo-rectal receiver coil would yield much higher signal sensitivity for the prostate. In addition, the air-filled balloon housing the endo-rectal coil would serve to immobilize the prostate, hence reducing motion induced image artifacts and blurring. Both of these features would be particularly useful for *in vivo* diffusion studies, especially diffusion anisotropy measurements. While these advantages are significant, the increased area of air/tissue interface encountered

when using an endo-rectal coil would likely introduce magnetic susceptibility related image artifacts in EPI based diffusion sequences. Localized shimming procedures and filling the ballon with susceptibility matching fluid, such as perfluro-carbon, would be helpful to alleviate the magnetic field inhomogeneity problem. Diffusion pulse sequences such as line-scan or fast spin-echo (33,35-37) could also be employed to reduced these susceptibility based artifacts.

No triggering was used with the single-shot EPI diffusion sequence in this study, although some study recommends pulse/cardiac gating (34). The single-shot nature of the acquisition and the motion correction procedures during post-processing minimizes the effect of bulk or slow body motion, while fast motion on the order of hundreds of milliseconds was not deemed significant for prostate. Considering the relatively distant location from the heart, the prostate is unlikely susceptible to pulsatile motion. Alternatively, respiratory gating or breath-hold acquisition can be practical for use with endo-rectal coil acquisition, where the decreased scan efficiency is compensated by the improved SNR.

Finally, to take advantage of the DTI contrasts quantitatively, six representative cases with different tumor burden are presented for *ex vivo* and *in vivo* (Fig. 6), respectively. The tumor volume and distribution were highlighted in bright orange in the volume rendered and projected DTI images using ADC threshold (mean tumor ADC + SD) and color coding, which correlate well with the corresponding histologically defined extent and stage for the same tumors.

In summary, we report diffusion properties, ADC and anisotropy, of histologically defined PCa *in vivo* and *ex vivo*. The good correlation between histology and volume rendered *in vivo* and *ex vivo* diffusion images suggests that the ADC threshold may provide a means for PCa volume estimation and tumor staging in peripheral zone tissue. Exploiting indices such as ADC and diffusion anisotropy is a valuable complement to conventional T2w imaging of the prostate.

Acknowledgment

We thank Mattew Budde to provide us the histology - *ex vivo* MRI co-registration software. The constructive comments from the reviewers are highly appreciately.

REFERENCES

1. Jemal A, Siegel R, Ward E, Murray T, Xu J, Smigal C, Thun MJ. Cancer statistics, 2006. CA Cancer J Clin 2006;56(2):106-130.
2. Kantoff PW, Rarroll PR, D'Amico AV, editors. Prostate Cancer: Principles & Practice. 1st ed. Philadelphia: Lippincontt Williams & Wilkins; 2002. 278-280 p.
3. Keetch DW, Catalona WJ, Smith DS. Serial prostatic biopsies in men with persistently elevated serum prostate specific antigen values. J Urol 1994;151(6):1571-1574.
4. Katz AE, Rewcastle JC. The current and potential role of cryoablation as a primary therapy for localized prostate cancer. Curr Oncol Rep 2003;5(3):231-238.
5. Guckenberger M, Flentje M. Intensity-modulated radiotherapy (IMRT) of localized prostate cancer: a review and future perspectives. Strahlenther Onkol 2007;183(2):57-62.
6. Cesaretti JA, Stone NN, Skouteris VM, Park JL, Stock RG. Brachytherapy for the treatment of prostate cancer. Cancer J 2007;13(5):302-312.
7. Rouviere O, Souchon R, Salomir R, Gelet A, Chapelon JY, Lyonnet D. Transrectal high-intensity focused ultrasound ablation of prostate cancer: effective treatment requiring accurate imaging. Eur J Radiol 2007;63(3):317-327.
8. Coakley FV, Qayyum A, Kurhanewicz J. Magnetic resonance imaging and spectroscopic imaging of prostate cancer. J Urol 2003;170(6 Pt 2):S69-75; discussion S75-66.
9. Kurhanewicz J, Swanson MG, Nelson SJ, Vigneron DB. Combined magnetic resonance imaging and spectroscopic imaging approach to molecular imaging of prostate cancer. J Magn Reson Imaging 2002;16(4):451-463.
10. Padhani AR, Gapinski CJ, Macvicar DA, Parker GJ, Suckling J, Revell PB, Leach MO, Dearnaley DP, Husband JE. Dynamic contrast enhanced MRI of prostate cancer: correlation with morphology and tumour stage, histological grade and PSA. Clin Radiol 2000;55(2):99-109.
11. Engelbrecht MR, Huisman HJ, Laheij RJ, Jager GJ, van Leenders GJ, Hulsbergen-Van De Kaa CA, de la Rosette JJ, Blickman JG, Barentsz JO. Discrimination of prostate cancer from normal peripheral zone and central gland tissue by using dynamic contrast-enhanced MR imaging. Radiology 2003;229(1):248-254.
12. Basser PJ, Pierpaoli C. Microstructural and physiological features of tissues elucidated by quantitative-diffusion-tensor MRI. J Magn Reson B 1996;111(3):209-219.

13. Song SK, Qu Z, Garabedian EM, Gordon JI, Milbrandt J, Ackerman JJ. Improved magnetic resonance imaging detection of prostate cancer in a transgenic mouse model. Cancer Res 2002;62(5):1555-1558.
14. Gibbs P, Tozer DJ, Liney GP, Turnbull LW. Comparison of quantitative T2 mapping and diffusion-weighted imaging in the normal and pathologic prostate. Magn Reson Med 2001;46(6):1054-1058.
15. Issa B. In vivo measurement of the apparent diffusion coefficient in normal and malignant prostatic tissues using echo-planar imaging. J Magn Reson Imaging 2002;16(2):196-200.
16. Chan I, Wells W, 3rd, Mulkern RV, Haker S, Zhang J, Zou KH, Maier SE, Tempany CM. Detection of prostate cancer by integration of line-scan diffusion, T2-mapping and T2-weighted magnetic resonance imaging; a multichannel statistical classifier. Med Phys 2003;30(9):2390-2398.
17. Hosseinzadeh K, Schwarz SD. Endorectal diffusion-weighted imaging in prostate cancer to differentiate malignant and benign peripheral zone tissue. J Magn Reson Imaging 2004;20(4):654.
18. Sato C, Naganawa S, Nakamura T, Kumada H, Miura S, Takizawa O, Ishigaki T. Differentiation of noncancerous tissue and cancer lesions by apparent diffusion coefficient values in transition and peripheral zones of the prostate. J Magn Reson Imaging 2005;21(3):258-262.
19. Pickles MD, Gibbs P, Sreenivas M, Turnbull LW. Diffusion-weighted imaging of normal and malignant prostate tissue at 3.0T. J Magn Reson Imaging 2006;23(2):130-134.
20. Kozlowski P, Chang SD, Jones EC, Berean KW, Chen H, Goldenberg SL. Combined diffusion-weighted and dynamic contrast-enhanced MRI for prostate cancer diagnosis--correlation with biopsy and histopathology. J Magn Reson Imaging 2006;24(1):108-113.
21. Gibbs P, Pickles MD, Turnbull LW. Diffusion imaging of the prostate at 3.0 tesla. Invest Radiol 2006;41(2):185-188.
22. Griswold MA, Jakob PM, Heidemann RM, Nittka M, Jellus V, Wang J, Kiefer B, Haase A. Generalized autocalibrating partially parallel acquisitions (GRAPPA). Magn Reson Med 2002;47(6):1202-1210.

23. Hasan KM, Parker DL, Alexander AL. Comparison of gradient encoding schemes for diffusion-tensor MRI. J Magn Reson Imaging 2001;13(5):769-780.
24. Shimony JS, Burton H, Epstein AA, McLaren DG, Sun SW, Snyder AZ. Diffusion tensor imaging reveals white matter reorganization in early blind humans. Cereb Cortex 2006;16(11):1653-1661.
25. Stejskal EO, Tanner JE. Spin diffusion measurements: spin echoes in the presence of a time-dependent field gradient. J Chem Phys 1965;42:288-292.
26. Humphrey PA, Vollmer RT. Intraglandular tumor extent and prognosis in prostatic carcinoma: application of a grid method to prostatectomy specimens. Hum Pathol 1990;21(8):799-804.
27. Xu J, Humphrey PA, Kibel AS, Snyder AZ, Narra VR, Song SK. ADC Decrease in Histology Identified Prostate Cancer. 2007; Berlin, Germany. p 3666.
28. Budde MD, Kim JH, Liang HF, Schmidt RE, Russell JH, Cross AH, Song SK. Toward accurate diagnosis of white matter pathology using diffusion tensor imaging. Magn Reson Med 2007;57(4):688-695.
29. Williams MC, Does MD, Price RR. ADC Mapping of Whole Excised Human Prostate. Proceedings of the International Society for Magnetic Resonance in Medicine 2004;12:2064.
30. Quint LE, Van Erp JS, Bland PH, Del Buono EA, Mandell SH, Grossman HB, Gikas PW. Prostate cancer: correlation of MR images with tissue optical density at pathologic examination. Radiology 1991;179(3):837-842.
31. Liney GP, Turnbull LW, Lowry M, Turnbull LS, Knowles AJ, Horsman A. In vivo quantification of citrate concentration and water T2 relaxation time of the pathologic prostate gland using 1H MRS and MRI. Magn Reson Imaging 1997;15(10):1177-1186.
32. Chen AP, Xu D, Henry R, Qayyum A, Kurhanewicz J, Vigneron DB. Diffusion Tensor Imaging of the Prostate Following Therapy. Proceedings of the International Society for Magnetic Resonance in Medicine 2003;11:579.
33. Vigneron DB, Xu D, Chen AP, Swanson MG, Kurhanewicz J. Diffusion Tensor Imaging of the Prostate using Single-Shot Fast Spin Echo. Proceedings of the International Society for Magnetic Resonance in Medicine 2002;10:457.

34. Sinha S, Sinha U. In vivo diffusion tensor imaging of the human prostate. Magn Reson Med 2004;52(3):530-537.
35. Reinsberg SA, Brewster JM, Payne GS, Leach MO, deSouza NM. Anisotropic Diffusion in Prostate Cancer: Fact or Artefact? Proceedings of the International Society for Magnetic Resonance in Medicine 2005;13:269.
36. Haker SJ, Szot Barnes A, Maier SE, Tempany CM, Mulkern RV. Diffusion Tensor Imaging for Prostate Cancer Detection: Preliminary Results from a Biopsy-Based Assessment. Proceedings of the International Society for Magnetic Resonance in Medicine 2005;13:2126.
37. Roebuck JR, Haker SJ, Tempany CM, Rybicki FJ, Maier SE, Mulkern RV. Diffusion Tensor Imaging of the Prostate: Low Anisotropies in Central Gland and Peripheral Zone in Men with Adenocarcinoma. Proceedings of the International Society for Magnetic Resonance in Medicine 2006;14:3338.
38. Meyer CR, Moffat BA, Kuszpit KK, Bland PL, McKeever PE, Johnson TD, Chenevert TL, Rehemtulla A, Ross BD. A methodology for registration of a histological slide and in vivo MRI volume based on optimizing mutual information. Mol Imaging 2006;5(1):16-23.

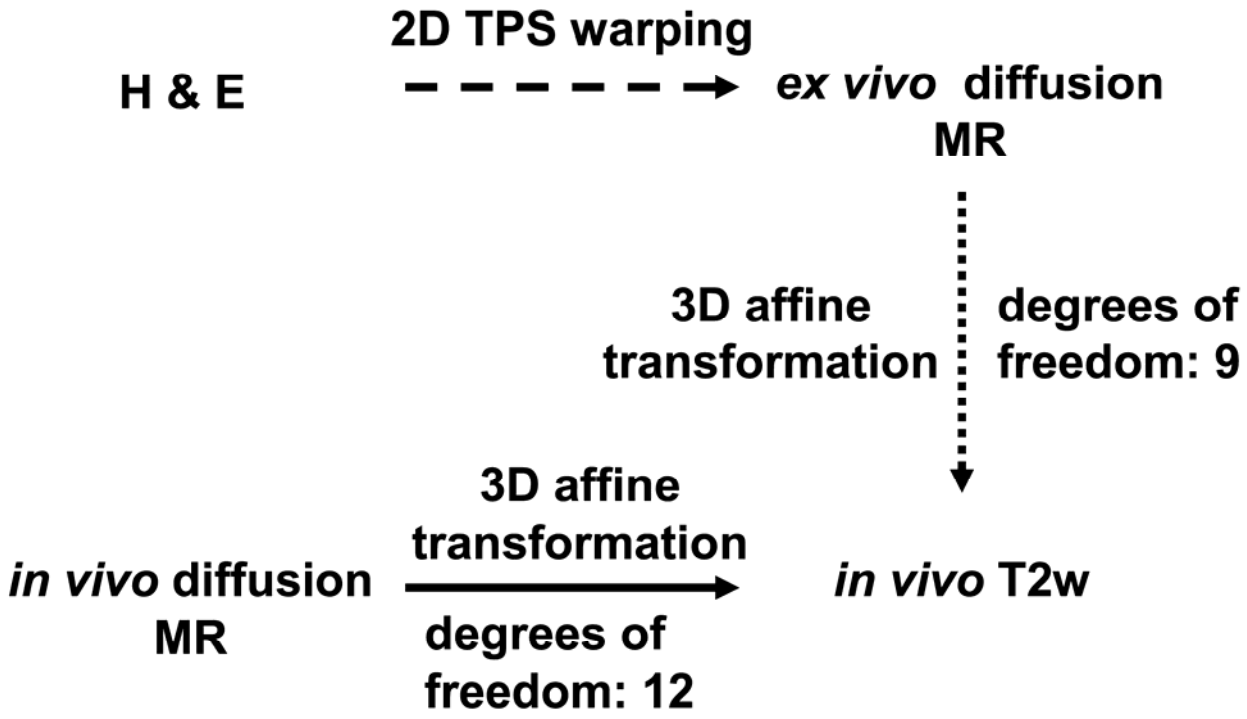

Figure 1. Overview of histology and MR co-registration scheme. The dashed line represents the semi-automatic thin plate spline (TPS) warping procedure using manually placed control points. The dotted line represents the manual image registration procedure to transform *ex vivo* coordinates into *in vivo* T2w coordinates. The solid line represents the unsupervised *in vivo* image co-registration procedure.

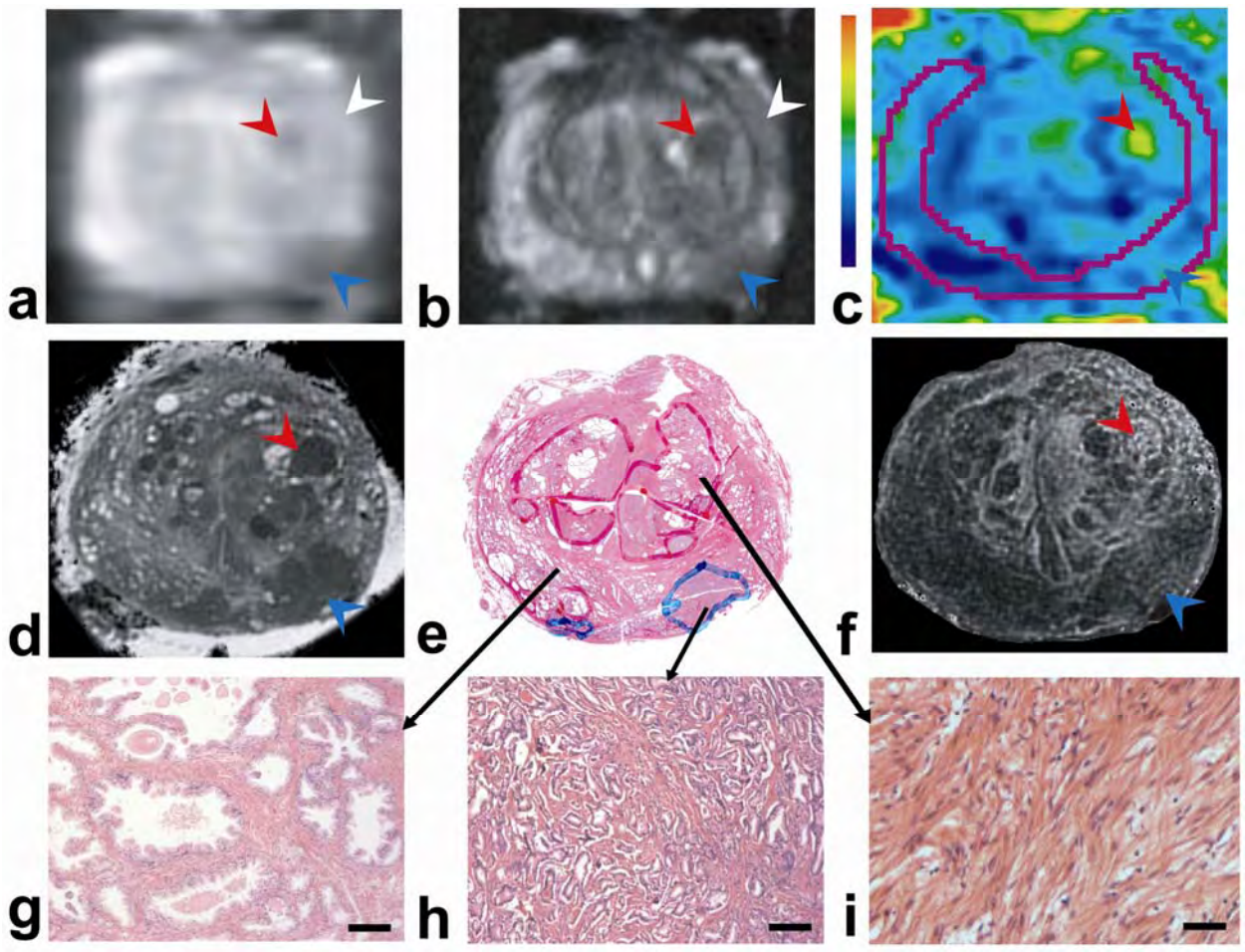

Figure 2. Co-registered images illustrate the tissue microstructure underpinning the MR diffusion characteristics. a) *in vivo* ADC (0 - 2.0 μm^2/ms), b) *in vivo* T2w, c) *in vivo* color coded FA (0 - 0.33), d) *ex vivo* ADC (0 - 2.0 μm^2/ms), e) H & E slide, and f) *ex vivo* FA (0 - 0.79). The cancerous and BPH regions in the H & E slide were marked in blue and red, respectively, by a urologic pathologist. Blue and red arrows indicate regions of PCa and stromal BPH, respectively, as diagnosed by histology. The white arrow in panel b indicates a T2 hypointense region that could be mistaken for PCa without the additional co-registered diffusion data. The peripheral zone region was delineated in panel b and mapped onto panel c in magenta. High resolution H & E examinations reveal the micro-structures of different types of tissues in g) benign peripheral zone, h) PCa, and i) stromal BPH (10× magnification, scale bar = 100 μm).

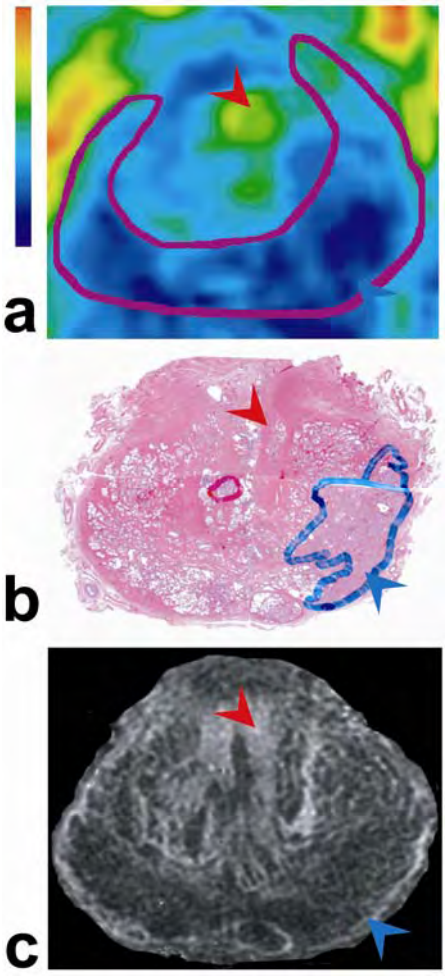

Figure 3. One representative case illustrates the lack of diffusion anisotropy differential between normal and cancerous tissue in the peripheral zone. The cancerous and BPH regions in the H & E slides were marked in blue and red, respectively, by a urologic pathologist. Red and blue arrows indicate regions of fibromuscular and carcinoma tissues, respectively, as identified by histology. a) *in vivo* FA map (0 - 0.33), b) H & E slide, and c) *ex vivo* FA map (0 - 0.79). The magenta line in b delineates the peripheral zone as in Fig. 2.

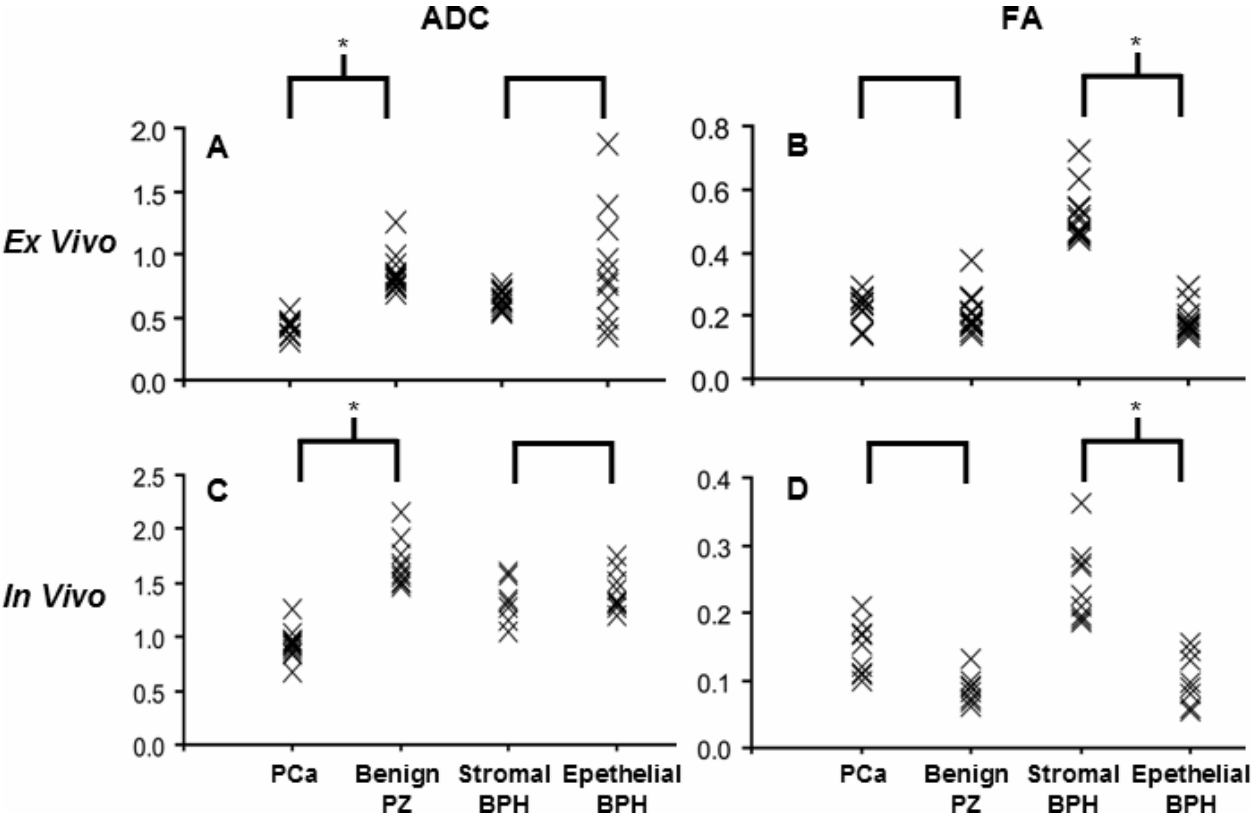

Figure 4. *Ex vivo* and *in vivo* ADC (μm^2/ms) and FA (unitless) values for each tissue type: (from left to right in each panel) PCa, benign PZ, stromal BPH, and epithelial BPH. * indicates significant differences ($p < 0.01$).

		ADC	FA	T2w
PZ	PCa	hypo	iso	hypo
	Benign	-	-	-
CG	PCa	hypo	iso	hypo
	Stromal BPH	hypo	hyper	hypo
	Epithelial BPH	hetero	iso	hetero
	Benign	-	-	-

Table 1. Tissue type classification combining DTI and T2w contrasts. Benign tissues (-) in PZ and CG, respectively, were used as benchmarks for MR contrasts. MR image contrasts were listed as hypo(intense), iso(intense), hyper(intense) or hetero(geneous).

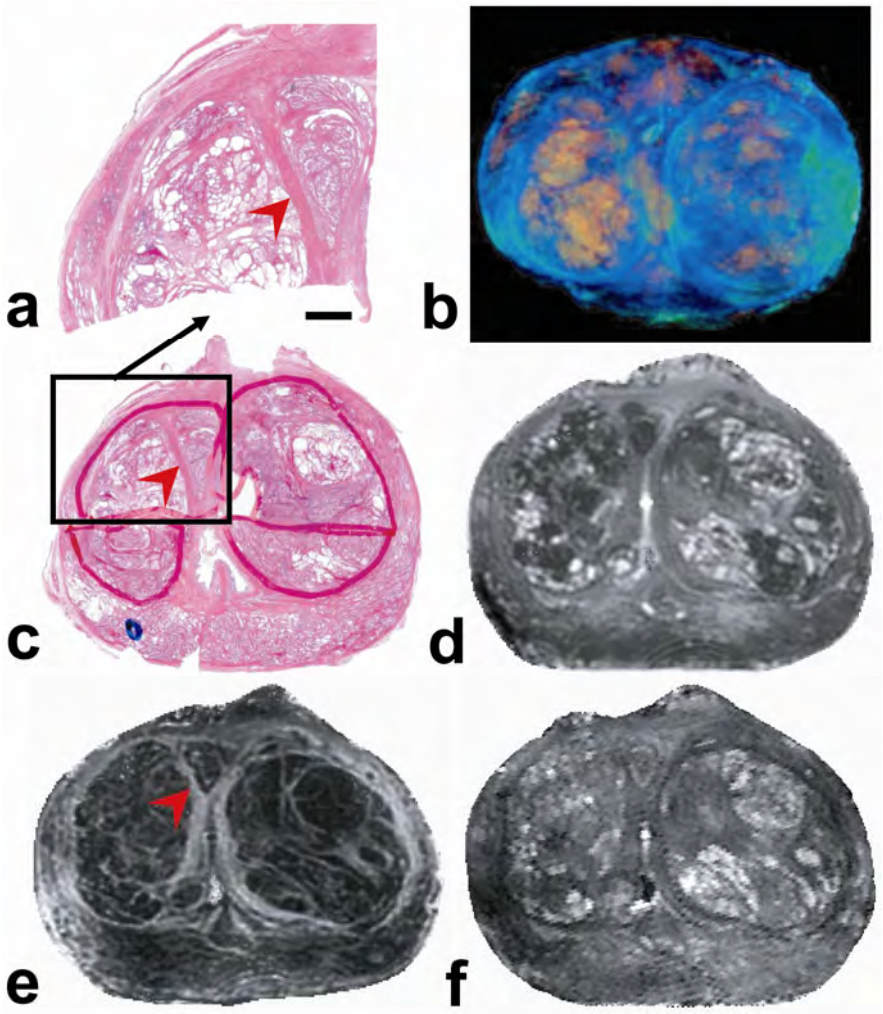

Figure 5. One representative case illustrates diffusion anisotropy delineation of BPH in prostate. The cancerous and BPH regions in the H & E slides were marked in blue and red, respectively, by a urologic pathologist. The region of BPH was largely composed of epithelial nodules with variable size and compactness. Red arrows indicate regions of bundled fibromuscular tissues, respectively, as identified by histology. a) magnified (scale bar = 3 mm) right anterior quadrant of the H & E slide, b) volume rendered *ex vivo* DTI image (image scale detailed in Fig. 5), c) H & E slide, d) *ex vivo* FA map (0 - 0.79), e) *ex vivo* ADC map (0 - 2.0 $\mu m^2/ms$), f) *ex vivo* T2w image.

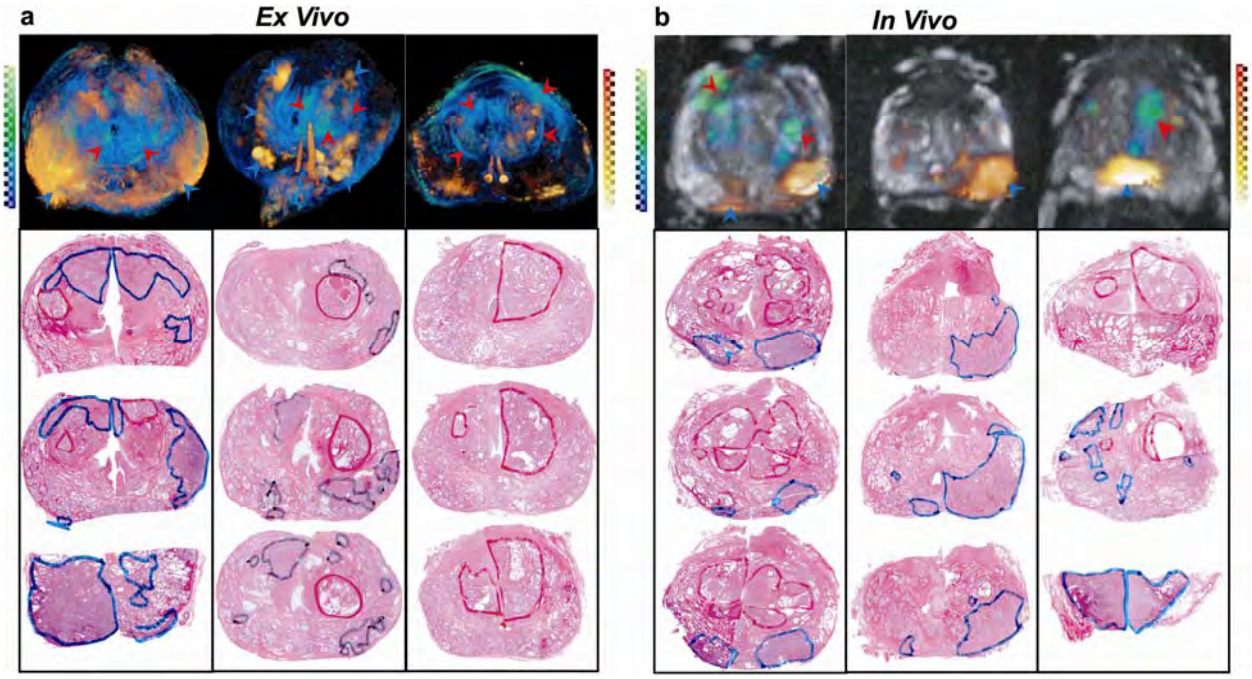

Figure 6. Diffusion tensor images were co-registered with step-sectioned histology slides from six representative specimens (each column) with different tumor sizes. PCa identified on the volume rendered DTI, *ex vivo* (panel a; projected view) and *in vivo* (panel b; projected view with a representative T2w image as background), closely correlated with those seen in histology. The histologically defined PCa extents and stages (from left to right in each panel) are 40% T3b, 16% T2c, and 4% T2c for *ex vivo*, and 15% T3a, 40% T3a, and 20% T3a for *in vivo*. The cancerous and BPH regions in the H & E slides were marked in blue/black and red, respectively, by a urologic pathologist. In the MR images, the ADC (0 - 0.50 μm^2/ms *ex vivo*, and 0- 1.15 μm^2/ms *in vivo*), and FA (0.39 - 1.0 *ex vivo*, and 0 - 0.41 *in vivo*) values were imported into the yellow-orange and green-blue channels, respectively. Bright yellow-orange regions in the MR images were identified as carcinoma determined by ADC threshold (*ex/in vivo* PCa mean ADC + SD). Red and blue arrows indicate regions of fibromuscular and carcinoma tissues, respectively, as identified by both the histology and the co-registered diffusion contrast in the MR images. In *ex vivo* DTI (panel a), pairs of ejaculatory ducts with high ADC value (color scale irrelevant) are segmented from the ADC map separately.

Magnetic Resonance Diffusion Characteristics of Histologically Defined Prostate Cancer in Humans

J. Xu[1], P. A. Humphrey[2], A. S. Kibel[3], A. Z. Snyder[4], V. R. Narra[4], J. J. Ackerman[1,4], and S-K. Song[4]

[1]Chemistry, Washington University, St. Louis, MO, United States, [2]Pathology & Immunology, Washington University, St. Louis, MO, United States, [3]Surgery, Washington University, St. Louis, MO, United States, [4]Radiology, Washington University, St. Louis, MO, United States

Introduction

The contrast provided by diffusion sensitive magnetic resonance (MR) in organ-confined human prostate cancer (PCa) offers the promise of improved detection and localization.[1] By employing an image co-registration procedures to align "gold standard" histology slide with *ex vivo*, and, subsequently, *in vivo* diffusion sensitive MR images,[2] the MR diffusion characteristics of histologically defined human prostate cancer were studied.

Material and methods

Patients Twelve radical prostatectomy patients (mean age 62 yrs, range 46 – 76 yrs) were enrolled in this study. *MRI* *In vivo* diffusion tensor imaging (DTI) (resolution = 2×2×2.5 mm^3) and T2-weighted (T2w) imaging (resolution = 1×1×2.5 mm^3) were performed prior to prostatectomy surgery. After surgery, prostatectomy specimens were fixed in formalin and step-sectioned at 4-mm intervals using a custom-made slicer. The regrouped 4-mm tissue blocks underwent ultra high resolution (0.5×0.5×0.5 mm^3) *ex vivo* DTI measurements.[3] *Histology* Individual 4-mm sections were carefully labeled and then completely embedded in paraffin and sampled in 4-μm thick slices for hematoxylin and eosin (H & E) staining. The histology slides and MR images were mutually aligned in the coordinate space of the standard *in vivo* T2w images.[2]

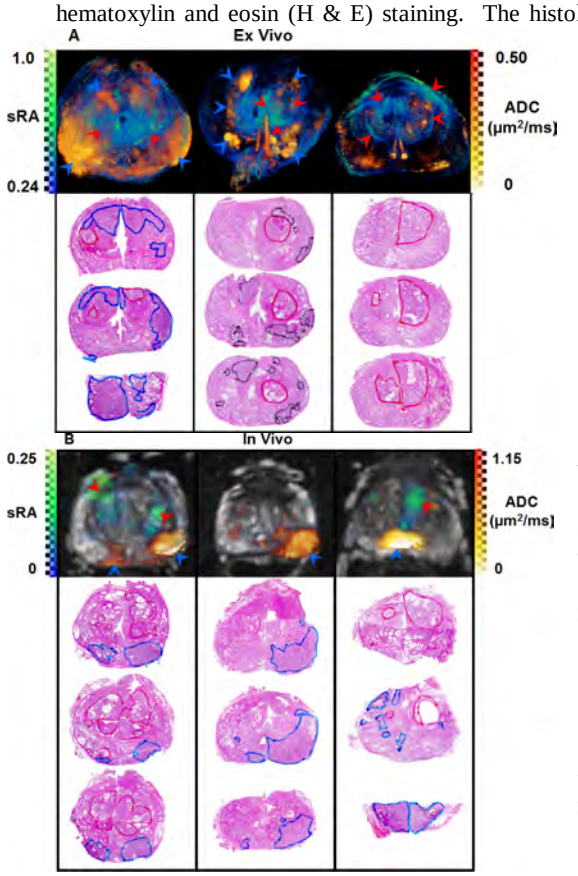

Figure 2. DTI images were co-registered with step-section histology slides from six representative specimens (each column) with different tumor sizes. PCa identified on the volume rendered DTI, *ex vivo* (panel A; projected view) and *in vivo* (panel B; projected view with a representative T2w image as background), closely correlated with those seen in histology. The histologically defined PCa extents and stages (from left to right in each panel) are 40% T3b, 16% T2c, and 4% T2c for *ex vivo*, and 15% T3a, 40% T3a, and 20% T3a for *in vivo*. The cancerous and BPH regions in the H & E slides were marked in blue/black and red, respectively, by a urologic pathologist. In the MR images, the ADC and diffusion anisotropy values were imported into the yellow-orange and green-blue channels, respectively. Bright yellow-orange regions in the MR images were identified as carcinoma determined by ADC threshold (*ex/in vivo* PCa mean ADC + standard deviation). Red and blue arrows indicate regions of fibromuscular and carcinoma tissues, respectively, as identified by histology and their co-registered diffusion contrast in the MR images. In *ex vivo* DTI images (panel A), pairs of ejaculatory ducts with high ADC value (color scale irrelevant) are segmented from the ADC map separately.

Results and Discussions

After MR and histology image co-registration for each slice, the PCa region and the benign tissue region in the peripheral zone (PZ) were translated from the histology slide (Fig. 1E) to both the *ex vivo* (Fig. 1D) and *in vivo* apparent diffusion coefficient (ADC) maps (Fig. 1A). The ADC value of PCa tissue (0.43 ± 0.06 $\mu m^2/ms$ *ex vivo*, Fig. 1D blue arrow, and 0.90 ± 0.13 $\mu m^2/ms$ *in vivo*, Fig. 1A blue arrow) was significantly lower than that of the non-cancerous PZ tissues (0.99 ± 0.16 $\mu m^2/ms$ *ex vivo*, and 1.66 ± 0.21 $\mu m^2/ms$ *in vivo*). Microscopically, normal prostate has a branching duct-acinar glandular architecture embedded in a dense fibromuscular stroma (Fig. 1G). This duct-acinar structure underlies the diffusion MR characteristics of the prostate gland in human. In prostate carcinoma, tightly packed tumor cells disrupt the duct-acinar structure leading to the decreased ADC in tumor due to the cellularity induced diffusion restriction (Fig. 1H). A relatively low diffusion anisotropy was observed in the PZ (scaled relative anisotropy or sRA = 0.13 ± 0.05 and 0.06 ± 0.03 for *ex vivo* and *in vivo*, respectively). The low diffusion anisotropy in the PZ likely reflects the random orientation of fibromuscular cells in the PZ (Figs. 1G and H). Importantly, no significant diffusion anisotropy differential was observed between the cancerous and non-cancerous PZ tissues (Figs. 1C and F, sRA = 0.13 ± 0.04 *vs.* 0.13 ± 0.03, p = 0.89 for *ex vivo*; and sRA = 0.08 ± 0.02 *vs.* 0.05 ± 0.02, p= 0.012 for *in vivo*). However, when the fibromuscular cells are bundled together at a length scale comparable to MRI voxel dimensions (Fig. 1I), higher diffusion anisotropy (sRA = 0.34 ± 0.08 *ex vivo* and 0.13 ± 0.06 *in vivo*) in those regions becomes distinctive and distinguishable (red arrows, Figs. 1C and F) from that in the glandular region. The appearance of BPH in ADC map or T2w image is very heterogeneous, reflecting the complicated BPH tissue composition. BPH regions with both ADC and T2w hypointensity could mimic PCa in the CG (Figs. 1A and B, red arrows), leading to false positive PCa identification. The high diffusion anisotropy in the bundled fibromuscular cells provides a unique contrast for differentiating these BPH nodules from PCa (Figs. 1C and F). Notably, the high diffusion anisotropy appears not only in the stromal components within BPH, but also in the fibrous tissues surrounding the BPH (Fig. 2A), as the expanding BPH nodule pushes and compacts the fibromuscular tissue network around it. This high diffusion anisotropy pattern surrounding the BPH was best visualized in the volume rendered DTI images (Fig. 2A, middle column, red arrows).

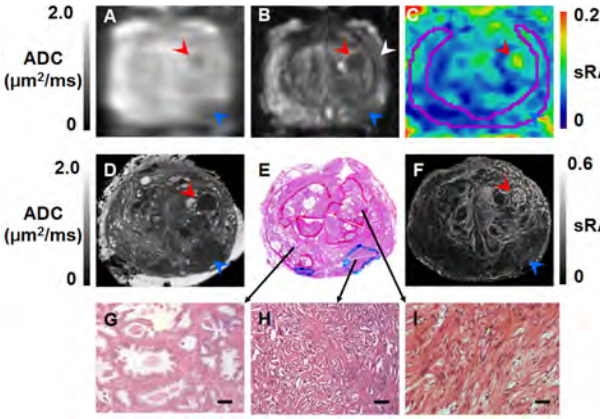

Figure 1. Co-registered images illustrate the tissue microstructure underpinning the MR diffusion characteristics. A) *in vivo* ADC, B) *in vivo* T2w, C) *in vivo* color coded sRA, D) *ex vivo* ADC, E) H & E slide, and F) *ex vivo* sRA. The cancerous and BPH regions in the H & E slide were marked in blue and red, respectively, by a urologic pathologist. Blue and red arrows indicate regions of PCa and stromal BPH, respectively, as diagnosed by histology. The white arrow in panel B indicates a T2 hypointense region that could be mistaken for PCa without the additional co-registered diffusion data. The peripheral zone region was delineated in panel B and mapped onto panel C in magenta. High resolution H & E examinations reveal the micro-structures of different types of tissues in G) benign peripheral zone, H) PCa, and I) stromal BPH (10× magnification, scale bar = 100 μm).

References [1] Pickles, *et al. JMRI* **23**, 130, 2006. [2] Xu, *et al. Proc. ISMRM.* **15**, 3666, 2007. [3] Xu, *et al. Proc. ISMRM.* **14**, 174, 2006.

ADC Decrease in Histology Identified Prostate Cancer

J. G. Xu[1], P. A. Humphrey[2], A. S. Kibel[3], A. Z. Snyder[4,5], V. R. Narra[4], and S-K. Song[4]

[1]Chemistry, Washington University in St. Louis, St. Louis, MO, United States, [2]Pathology & Immunology, Washington University in St. Louis, St. Louis, MO, United States, [3]Surgery, Washington University in St. Louis, St. Louis, MO, United States, [4]Radiology, Washington University in St. Louis, St. Louis, MO, United States, [5]Neurology, Washington University in St. Louis, St. Louis, MO, United States

Introduction

The ability to accurately localize prostate carcinoma (PCa) within prostate gland non-invasively can dramatically improve PCa diagnosis and treatment. However, conventional T2 weighted (T2W) imaging has not proven sensitive or specific enough to localize gland-confined PCa. Recently substantial decrease of mean water apparent diffusion coefficient (ADC), due to disruption of the prostate ductal structures by PCa, provides a unique contrast for tumor localization. This promising ADC contrast has been explored *in vivo*, as recently summarized by Pickles *et al.* [1]. Nevertheless, none of the reports to date validated the suspected PCa region, either diagnosed by T2W, ADC contrast, or biopsy, with the "gold standard" histology. Herein, we propose a co-registration strategy to determine the *in vivo* ADC of histology identified PCa.

Material and methods

Patients Twelve radical prostatectomy patients (mean age 62 yrs, range 46 – 76 yrs) without any preoperative treatment were enrolled in this study.

MRI *In vivo* diffusion tensor imaging (DTI) measurement (resolution = 2×2×2.5 mm) and T2W imaging (resolution = 1×1×2.5 mm) were performed prior to scheduled prostatectomy surgery [2]. After surgery, prostatectomy specimens were fixed in formalin for more than 24 hours and step-sectioned at 4-mm intervals using a custom-made slicer. The regrouped 4-mm tissue blocks underwent ultra high resolution (0.5×0.5×0.5 mm) *ex vivo* DTI measurement [3].

Histology Individual 4-mm sections were carefully labeled to ensure correct identification of each section within the prostate. The sectioned slabs were then completely embedded in paraffin and sampled in 4-μm thick slices for hematoxylin and eosin (H & E) staining. Regions of PCa and BPH were identified and outlined in blue and red, respectively, by a urologic pathologist.

Image registration A two-dimensional (2D) thin plate spline (TPS) warping was performed using 10 – 20 control points (Fig 2, A and B) to transform histology to the coordinate of *ex vivo* ADC map (Fig. 1, T1). By using a rigid body 3D affine transformation (Fig. 1, T2), the *ex vivo* ADC maps were further manually co-registered with the *in vivo* T2W images through intra-glandular structure alignment. The *in vivo* ADC maps were also co-registered with the *in vivo* T2W images using a 3D affine transformation (Fig. 1, T3). In this manner, all the images were mutually aligned in the coordinate space of the standard *in vivo* T2W images.

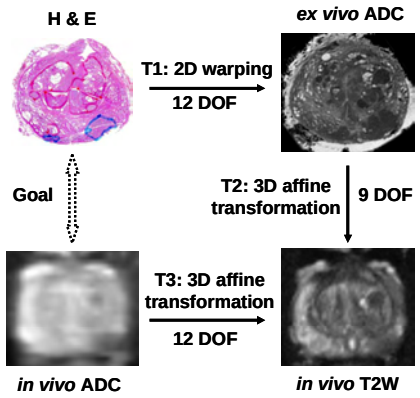

Figure 1. Overview of histology and *in vivo* ADC co-registration.

Results and Discussions

The ultra high resolution *ex vivo* diffusion anisotropy map (Fig. 2B), revealing exquisite intra-glandular structure, affords accurate placement of the control points in the corresponding histology slide (Fig. 2A). The *ex vivo* ADC map, exhibiting similar tissue contrast as the *in vivo* T2W images, provides a critical link to the *in vivo* ADC map. Excellent co-registration results were achieved despite some manual procedures involved (Fig. 3). The registration results may be further improved by utilizing mutual information based automatic procedures [4]. After image registration, cancerous (Fig. 2D) and normal (Fig. 2C) tissues in the PZ were mapped from the histology slides onto the *in vivo* and *ex vivo* ADC maps to determine the ADC values in each tissue category. The ADC values in PCa is consistently much lower than that in normal tissues (Fig. 4) in *in vivo* patients, *ex vivo* prostatectomy specimens, and an *in vivo* mouse model of PCa [5].

Reference [1] Pickles, *et al. J. Magn. Reson. Imaging* **23**, 130, 2006. [2] Xu, *et al. Proc. Intl. Soc. Magn. Reson. Med.* **13**, 2125, 2005. [3] Xu, *et al. Proc. Intl. Soc. Magn. Reson. Med.* **12**, 2508, 2004. [4] Meyer, *et al. Mol. Imaging* **13**, 16, 2006. [5] Song, *et al. Cancer Res.* **62**, 1555, 2002.

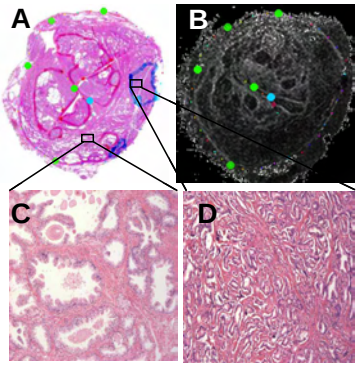

Figure 2. Representative control points that drive the 2D TPS warping in the T1 transformation are enlarged in both the H&E slide (A) and the *ex vivo* diffusion anisotropy map (B). Cancerous (marked blue in A) and non-cancerous PZ, identified by pathologist, are magnified to show the more cellular PCa (D) comparing to the normal ductal tissues (C).

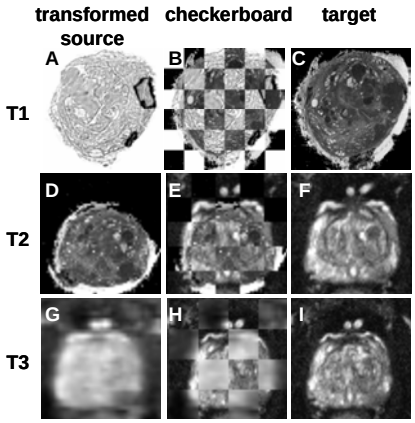

Figure 3. Registration results at three transformation stages (rows, T1 - T3). The transformed source images (left column) were overlaid onto the target images (right column) to highlight alignment results in checkerboards (center column). The transformation pairs are A) TPS warped H&E and C) *ex vivo* ADC; D) transformed *ex vivo* ADC and F) *in vivo* T2W; and G) transformed *in vivo* ADC and I) *in vivo* T2W.

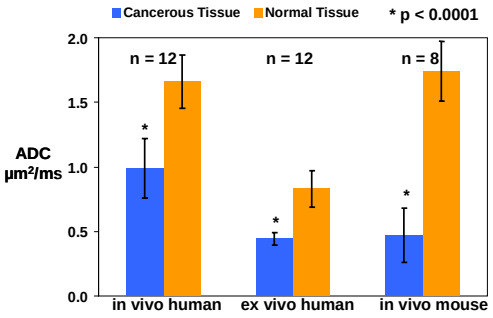

Figure 4. Decreased ADC values were observed in *in vivo* patients, *ex vivo* human prostatectomy specimens, and an *in vivo* mouse model of PCa. All results were determined by histopathology identified tissue categories. Error bars represent mean standard deviation. Statistical significance was accepted for $p < 0.0001$.

Exclusion of False Positive Identification of Prostate Cancer Using Diffusion Anisotropy

J. G. Xu[1], P. A. Humphrey[2], A. S. Kibel[3], V. R. Narra[4], S-K. Song[4]

[1]Chemistry, Washington University in St. Louis, St. Louis, Missouri, United States, [2]Pathology & Immunology, Washington University in St. Louis, St. Louis, Missouri, United States, [3]Surgery, Washington University in St. Louis, St. Louis, Missouri, United States, [4]Radiology, Washington University in St. Louis, St. Louis, Missouri, United States

Introduction

The normal prostate comprises a branching duct-acinar glandular system embedded in a dense fibromuscular stroma. The substantial decrease of mean water diffusivity due to disruption of the ductal structures by prostate cancer (PCa) provides unique contrast for tumor localization. However, it is difficult to distinguish PCa from benign prostatic hyperplasia (BPH) on the basis of changes in mean diffusivity alone because both processes affect this diffusion parameter. An alternative means of distinguishing PCa and BPH is through measures of diffusion anisotropy, which has not yet been systematically evaluated in this role. To examine the potential utility of diffusion anisotropy for PCa identification, the prostates from thirteen radical prostatectomy patients were examined by diffusion tensor imaging (DTI) *in vivo* before surgery, and *ex vivo* after surgery and formalin fixation. DTI findings were validated by co-registered histology.

Material and methods

MRI *In vivo* DTI was performed on a 1.5-tesla scanner using a phased-array body coil at 2 × 2 × 2.5 mm resolution. Diffusion sensitizing gradients were applied along six directions. Two diffusion sensitizing factors or *b* values = 0 and 500 s/mm^2 were used to calculate the apparent diffusion coefficient (ADC) and scaled relative anisotropy (sRA). Additionally, fat saturated T_2 weighted (T2W) images were acquired at 1 × 1 × 2.5 mm resolution. After surgery, prostatectomy specimens were fixed in formalin for more than 24 hours and step-sectioned at 4-mm intervals. The 4-mm sections were regrouped with a thin sheet of susceptibility matched spacer inserted between adjacent sections for MRI slice prescription. Ultra high resolution (0.125 mm^3 voxel size) *ex vivo* DTI, employing parameters reported previously [1], was performed on the regrouped slices.

Histology Individual 4-mm sections were carefully labeled to ensure correct identification of each section within the prostate. The sectioned slabs were then completely embedded in paraffin and sampled in 4 μm thick slices for hematoxylin and eosin (H & E) stains. Regions of PCa and BPH were identified and outlined in blue and red, respectively, by a urologic pathologist. The diffusion weighted (DW) images obtained *in vivo* were co-registered with the higher resolution *in vivo* T2W images, then with the even higher resolution *ex vivo* DW images, and finally with the optical microscopy images using algorithms based on 3D affine transformation and normalized mutual information.

Results and Discussions

The expanding nodules of BPH push and tighten the normal fibromuscular system around them, resulting in ordered fiber bundles with networked structure in the sRA map (Fig. 1 A). Diffusion anisotropy was higher in these ordered, compressed areas (0.34 ± 0.08, Figs. 1 B – D) compared to that of the acinar glandular tissues and PCa, for which sRA was 0.13 ± 0.05 *ex vivo* (n = 13, $p < 0.001$). A similar differential holds for *in vivo* diffusion anisotropy measures. sRA values were 0.13 ± 0.07 for fibromuscular tissue compared with 0.05 ± 0.02 for glandular tissue and PCa (n = 13, $p < 0.001$). The sRA for both types of tissues are smaller *in vivo* than *ex vivo* due to the lower image resolution and the resulting partial volume effects for the *in vivo* data. We found that diffusion anisotropy remains low both *in vivo* and *ex vivo* in the glandular tissues regardless of the presence of PCa, as also noted by Reinsberg *et al.* [2]. In light of our preliminary experimental observations and the expected tissue microstructure changes, we propose that high diffusion anisotropy can be used as an exclusion criterion for PCa diagnosis. As noted above, areas of BPH may exhibit PCa-like contrast on both the T2W images (black arrow, Fig. 2 A) and ADC maps (black arrow, Fig. 2 B), which could lead to a false positive diagnosis. In all three patients with BPH mimicking PCa, the presence of elevated diffusion anisotropy (black arrow, Fig 2 C) reliably prevents a false positive identification of PCa. The validity of this identification was confirmed by the corresponding histology (Fig. 2 D). In the representative case shown here, the area of reduced ADC (black arrow, Figs. 2 A – D) corresponds to a stromal BPH nodule (Figs. 2 E - F). Despite the much smaller diffusion anisotropy magnitude and differential *in vivo*, the presence of elevated anisotropy was sufficient to prevent misidentification of BPH as PCa.

Reference [1] Xu, *et al. Proc. Intl. Soc. Mag. Reson. Med.* **12**, 2508, 2004. [2] Reinsberg, *et al. Proc. Intl. Soc. Mag. Reson. Med.* **13**, 269, 2005.

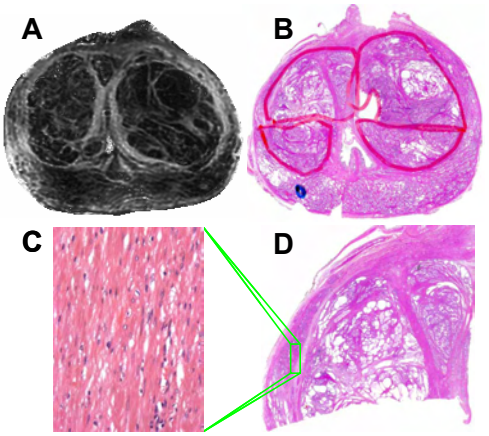

Figure 1. Corresponding *ex vivo* sRA map (A) and H & E stains (B) with PCa and BPH outlined in blue and red, respectively. The high diffusion anisotropy region in the top left quadrant of the histology slide (D) was further examined at 20 × magnification (C).

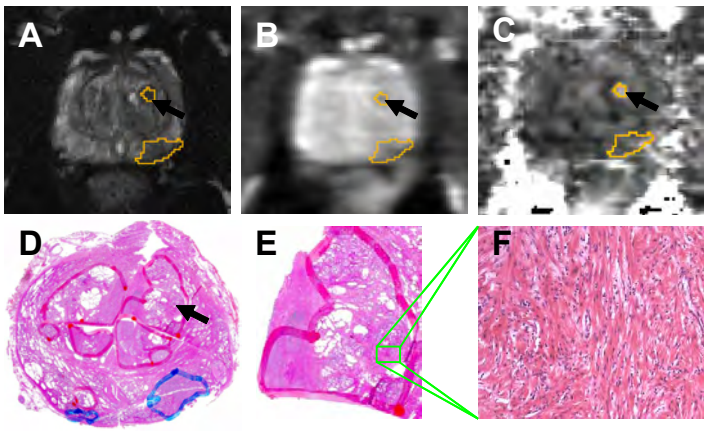

Figure 2. Corresponding *in vivo* T2W image (A), ADC map (B), sRA map (C), and H & E stains (D) with PCa and BPH outlined in blue and red, respectively. Using ADC contrast only, the suspected PCa regions were outlined in orange (B) and mapped onto the T2W image (A) and sRA map (C). The high diffusion anisotropy region (black arrow) was histologically verified as a BPH nodule (E), with its stromal structure revealed at 20 × magnification (F).